Eur. J. Mineral.
2002, **14**, 203-224

An introduction to the use of neutron scattering methods in mineral sciences

MARTIN T. DOVE*
Department of Earth Sciences, University of Cambridge, Downing Street, Cambridge CB2 3EQ, UK

Abstract: We review the current state of the field of neutron scattering as applied to studies of mineral behaviour. Neutron scattering is a particularly versatile tool because it is able to measure both structure (diffraction) and dynamics (spectroscopy) of materials at an atomic level, and because it is able to measure both coherent and incoherent scattering processes. As a result, there is a wide range of phenomena that can be studied using neutron scattering. The versatility of the tool is shown to arise within a general theoretical framework. Applications of neutron scattering in the Earth and Mineral Sciences are described.

Keywords: Neutron scattering, inelastic neutron scattering, diffuse scattering, total scattering, diffraction, incoherent neutron scattering, quasi-elastic neutron scattering.

1. Introduction

1.1 Neutron scattering as an emerging tool in Earth and Mineral Sciences

Until recently neutron scattering methods had been applied only sporadically to problems in the Earth and Mineral Sciences. The current growing interest in the use of neutron scattering in this field is partly due to the development of improved neutron sources, such as the UK ISIS pulsed neutron source, and the development of new methods and instrumentation. With regard to instrumentation, exciting developments have been facilitated by the possibility for vastly increase coverage by huge banks of detectors, with high-throughput data handling capabilities which have been increased by developments in computing, data storage and communications. Examples are the GEM general-purpose diffractometer and MAPS magnetic excitations spectrometer at ISIS (the best source of information is the ISIS web site, http://www.isis.rl.ac.uk/). New instruments give rise to new science possibilities, some of which have led to the growing interest in mineral sciences applications of neutron scattering. These include possibilities for diffraction studies of complex minerals with subtle phase transitions, high-pressure studies, and spectroscopic studies. With the prospects of more advanced neutron sources coming on line over the next decade, including upgrades of ISIS (such as the development of a second target station), the SNS pulsed source at Oak Ridge (USA), and possibly the European ESS pulsed source, with the new opportunities these will give, it is timely to review the present state of the art in applying neutron scattering methods to solve problems in minerals sciences. Some of the possibilities for the future have been reviewed by Artioli *et al.* (1996a).

1.2 The interaction of neutrons with matter

Properties of the neutron

The neutron provides a unique probe of the atomic properties of matter. It carries no charge, and has a magnetic moment. Because it has no charge, and unlike electromagnetic radiation and electrons, the neutron does not interact with the atomic charge distribution. Instead, the neutron interacts *via* the strong nuclear force with the atomic nucleus, and *via* its magnetic moment with the magnetisation density fluctuations (spatial and temporal) of the atoms. The mass of the neutron (1 a.m.u.) is similar to the masses of atomic nuclei (*i.e.*, from 1–240 a.m.u.). This means that the momentum and energy of a neutron can be similar to the momenta and energies of atoms in normal matter. Furthermore, the wavelength of a beam of neutrons will be similar to interatomic spacings. As a result, neutron beams can be used as probes of both structure and dynamics of materials, as will be highlighted in this review and in other reviews in this collection. This includes crystal structure and phonon dynamics, which are concerned with the atoms, and magnetic structures and magnetic excitations.

There are two types of processes in which neutrons interact with matter, namely *neutron scattering* and *neutron absorption*. The interaction of the neutron with matter, whether through scattering or absorption, is usually quite

*e-mail: martin@esc.cam.ac.uk

DOI: 10.1127/0935-1221/2002/0014-0203
0935-1221/02/0014-0203 $ 9.90

weak, although there are notable (and generally useful) exceptions. This is in contrast with other probes such as conventional X-ray diffraction.

The strength of the scattering from an atomic nucleus is defined in either of two ways. The *first* is the formal equivalence of the atomic scattering factor, which for neutron scattering is called the *scattering length* (and with units of length), and it is usually given the symbol b. The *second* definition is as a scattering cross section with symbol σ (and with units of area). By convention, the cross section is linked to the scattering length by $\sigma = 4\pi b^2$. The use of the scattering cross section is useful for comparing different types of interaction between the neutron and the nucleus.

Neutron scattering processes

The scattering interaction between the neutron and atomic nucleus takes place over extremely short length scales, of the order of 10^{-15} m. By contrast, the interaction between X-rays and the atomic charge distribution operates at the length scale of the atom, namely around 10^{-10} m (1 Å). The amplitude of a scattered beam of radiation varies with scattering vector Q as the inverse of the size of the length scale involved in the scattering process. For X-ray diffraction, this means that there is a considerable reduction in the amplitude of scattering over the range of values of Q in a typical experiment (*e.g.*, 0–6 Å^{-1}). On the other hand, the small distances involved in neutron scattering mean that there is no appreciable change in the scattering length over the same range of Q. Together with the high resolution now possible with neutron powder diffraction instrumentation, the independence of the scattering length on Q has helped neutron powder diffraction to become particularly valuable in determining crystal structures of minerals and the variation of structure with changing temperature and/or pressure. This is important because the crystal structures of minerals can be relatively complicated in comparison with other inorganic crystals. Neutron powder diffraction is now an established tool for the study of subtle changes in structure associated with phase transitions, as reviewed by Pavese (2002) and Redfern (2002).

Unlike nuclear scattering, the scattering of neutrons by the magnetic moments of atoms does have a significant dependence on Q. The magnetisation of an atom arises from the unpaired electrons in the atoms, and the magnetisation density extends across the same length scale as the charge distribution. This means that the scattering length for magnetic scattering varies with Q in a manner similar to that for X-ray scattering.

There are two main types of neutron scattering processes. The *first* is *coherent scattering*, which is the scattering process in which the scattering from each atom of the same type is independent of the nuclear isotope and spin state. In effect, coherent scattering processes average over isotope number and spin state. The *second* type of interaction is *incoherent scattering*, which accounts for differences in scattering from atoms of the same type due to differences in isotope or spin state. Clearly, any atom with a nucleus of zero spin and with only one isotope will have a zero incoherent cross section. The separation of coherent and incoherent scattering processes is described in more detail in §2.2.

Neutron scattering cross sections are actually relatively weak. Unfortunately, this is coupled with the fact that even the most advanced neutron sources have relatively low fluxes of neutrons as compared to X-ray, laser or electron radiation sources (see Winkler, 2002, for a discussion of sources of neutrons). This means that neutron scattering experiments may be time consuming, and the high costs of producing and detecting a neutron beam (Winkler, 2002) mean that neutron scattering experiments are relatively expensive. However, these negative points are more than offset by the unique information that can be given by neutron scattering, as will be highlighted in this and the other reviews in this collection of papers.

Neutron absorption processes

The other type of interaction between neutrons and atomic nuclei is *absorption*. In many cases, the cross section of neutron absorption is quite low. However, there are some nuclei that have relatively large absorption cross sections. These can occur either as resonances, or as an absorption process that varies as the inverse of the neutron velocity. Two examples of common neutron-absorbing materials are boron and cadmium. Both of these are often used in neutron scattering experiments because of their absorbing power, usually as components to mask the trajectory of the incoming and scattering neutron beam in order to avoid measurements of neutrons scattering from elsewhere other than the sample.

The low absorption of neutron beams passing through most materials means that neutrons can penetrate through the walls of sample environment equipment. This facilitates the development of such equipment without needing to compromise the quality of the types of experiment that can be performed. For example, good control at high and low temperatures is a routine operation in a neutron scattering experiment (Pavese, 2002; Redfern, 2002). Traditionally, high pressures have been easier to work with using X-ray diffraction and diamond anvil cells, but the use of time-of-flight neutron scattering techniques (Winkler, 2002) have facilitated considerable progress in neutron scattering at high pressures (Besson & Nelmes, 1995). It is now also possible to perform neutron diffraction measurements at simultaneous high pressures and temperatures (Zhao *et al.*, 1999, 2000; Le Godec *et al.*, 2001, 2002), as reviewed by Redfern (2002).

The usually low absorption of neutron beams also means that neutrons will interact with the bulk of the sample under study. In some circumstances, there can be measurable differences between the behaviour of a material at its surface and the behaviour in the bulk (displacive phase transitions most often give this effect). In such cases, conventional X-ray and neutron diffraction experiments may give different results if the results of a conventional X-ray diffraction experiment are dominated by scattering from the surface.

Neutron absorption processes are essential for the operation of neutron detectors. Common absorbing materials in

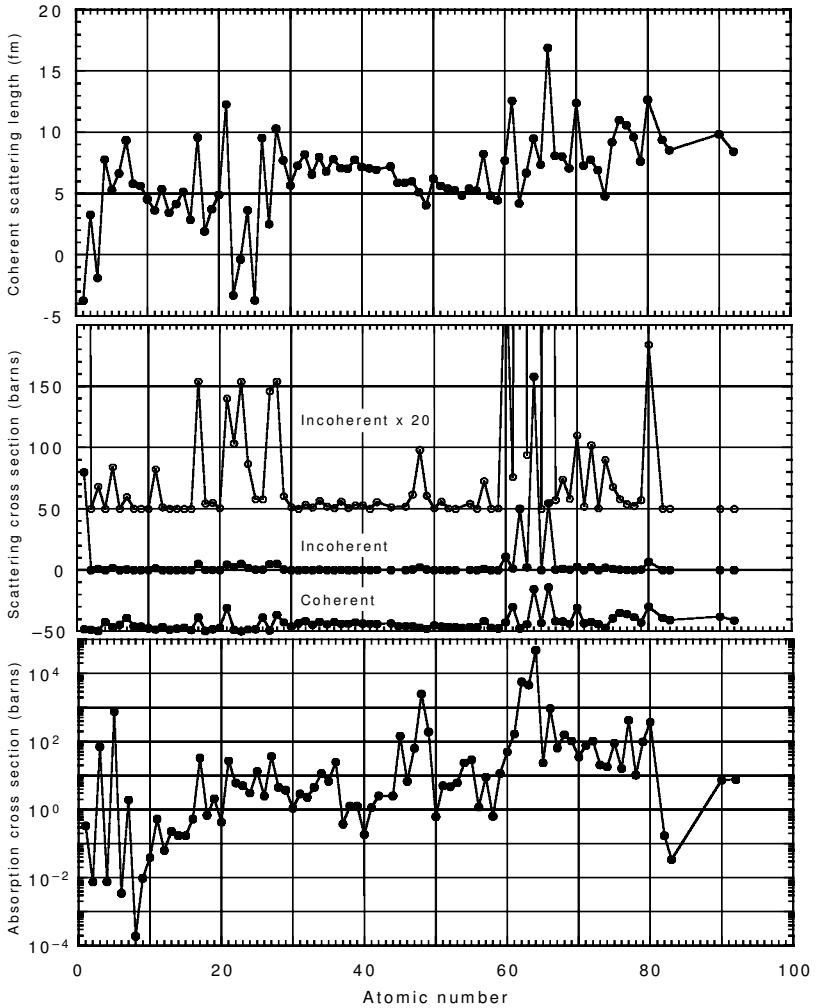

Fig. 1. *Top*, dependence of coherent neutron scattering lengths on atomic number. *Middle*, comparison of the coherent and incoherent scattering cross sections for the same range of atomic number. For clarity, the plot of the coherent scattering cross sections has been lowered by 50 barns, and a raised plot of incoherent scattering cross sections multiplied by 20 is also included. *Bottom*, logarithmic plot of neutron absorption cross sections. Among the important features of these diagrams are the large incoherent cross section and negative coherent scattering length for hydrogen (atomic number 1); the near-zero value of the coherent scattering length of vanadium (atomic number 23) with an appreciable cross section for incoherent scattering; the relatively large absorption cross sections of boron (atomic number 5), cadmium (atomic number 48) and gadolinium (atomic number 64), each of which can be used to provide neutron shielding for precision experiments; contrast between the coherent scattering lengths of important isoelectronic (or nearly isoelectronic) atoms, such as the Mg/Al/Si and Mn/Fe/Co/Ni series. Data are from V.F. Sears, as quoted in Bée (1988).

neutron detectors are lithium and ^{3}He. Boron (in the gaseous compound BF_3) and gadolinium are also used as neutron absorbing materials in neutron detectors (see Winkler, 2002).

Resonance absorption of neutrons can be exploited in the design of experiments. Fowler & Taylor (1987) proposed that measurements of the absorption resonance profile could be used to measure the temperature of a sample, through the Doppler broadening of the resonance line (see also Mayers *et al.*, 1989, Frost *et al.*, 1989). This procedure has recently been exploited for the measurement of temperature in diffraction experiments at simultaneous high pressures and temperatures, where thermocouples would be difficult to use (Le Godec *et al.*, 2001, 2002).

Neutron absorption processes can also be exploited for macroscopic imaging and tomographic studies of mineral and melt properties, as reviewed by Winkler *et al.* (2002).

Variation with atomic number

Neutron scattering and absorption cross sections do not vary systematically with atomic number (although there are some general trends, albeit with very large fluctuations away from these trends). The variation with atomic number of the coherent scattering lengths, incoherent scattering cross sections, and neutron absorption cross sections are illustrated in Fig. 1. Several important features emerge from a consideration of the data in Fig. 1.

It can be noted that there are interesting contrasts in the coherent scattering lengths for groups of atoms or ions with similar numbers of electrons, such as Mg^{2+}, Al^{3+} and Si^{4+}. These will have very similar scattering cross sections for X-ray diffraction, but significantly different scattering lengths for neutron diffraction. In fact, there are some atoms, including ^{1}H, Mn, and Ti, that have negative coherent scattering lengths. In these cases, the phase of the scattered neutron beam is reversed compared to the phase when scattering from atoms with positive scattering length. This will increase the difference between the scattering lengths of similar atoms even further.

In Fig. 1 we compare the coherent and incoherent scattering cross sections for all atoms. It can be seen that for most atoms the coherent scattering cross section is the larger of the two, which is essential for the study of structure through diffraction and for measurements of collective excitations. However, there are some nuclei for which the cross section for incoherent scattering is particularly large. ^{1}H is one of these nuclei. In a powder diffraction experi-

ment on a hydrous mineral, the incoherent scattering from the hydrogen nucleus can give a large contribution that dominates the diffraction pattern for all values of Q, which effectively limits the accuracy of the information that can be extracted from the diffraction pattern. However, the deuterium nucleus has a zero incoherent scattering cross section, and the problem associated with hydrogen can be eliminated if the hydrogen atoms in the sample to be studied can be completely replaced by deuterium.

Figure 1 also shows the wide range of neutron absorption cross sections. The relatively large absorption cross sections of some nuclei, such as lithium ($Z = 3$) and boron ($Z = 5$), can be seen to be several orders of magnitude larger than for atoms with similar mass. Lithium and boron are used in neutron detectors, and boron is also used in shielding materials.

1.3 Neutron scattering and the Earth and Mineral Sciences

Rinaldi (2002) has reviewed a wide range of reasons why neutron scattering is of direct interest to the Earth and Mineral Sciences. We have highlighted above the issues of sensitivity to nuclei of similar atomic number and the ability to study magnetic minerals, and the possibility to study both structure and dynamics.

The wide range of particular advantages of neutron scattering listed above and in Rinaldi (2002), can be encapsulated in the fact that neutron scattering methods have an astonishing versatility. This versatility arises from the properties of the neutron. In particular, the wavelengths and energies of neutrons are comparable to the length and energy scales of the atoms in solids and fluids. This contrasts with X-rays, where the wavelength is similar to the interatomic spacings but the energy is several orders of magnitude higher than the energy of lattice vibrations. Laser light and infrared radiation have energies closer to atomic vibration energies, but their wavelengths are much larger than interatomic spacings. Since neutron scattering probes both the length and energy scales of atomic processes, it is possible to design experiments that focus on both spatial and dynamic processes at the same time, or else which focus on one or other. We will formalise this versatility below.

The versatility of neutron scattering methods can be illustrated with reference to the hydrogen atom. Many minerals contain hydrogen, sometimes in the form of bound or free hydroxide ions, and sometimes in the form of bound water molecules or as free water molecules within cavities in the crystal structure. X-rays are very insensitive to hydrogen, but neutrons are scattered by both hydrogen, ^{1}H, and deuterium, ^{2}H, nuclei. Hydrogen ^{1}H has an extremely large cross section for incoherent scattering – this is the cross section for neutron scattering that can be used to study the motions of *individual* hydrogen atoms (§4). Slow motions of the hydrogen atoms, whether in translational diffusion or reorientational motions of molecules containing hydrogen atoms, can be probed by *quasi-elastic incoherent scattering* (§4.2, 4.4), and fast motions of individual atoms, as in lattice or molecular vibrations, can be studied by high-energy spectroscopy (§4.3). On the other hand, since deuterium has a reasonable cross section for coherent scattering and no appreciable cross section for incoherent scattering, deuterated samples can be used in diffraction studies for the location of hydrogen sites in crystal structures or in studies of individual collective excitations.

The objective of this article is to review the formalism of neutron scattering, and to highlight how the formalism leads to the versatility and the great diversity of applications of the methods for studies in mineral sciences. We will start with the general formalism, and show how it can be separated into several different components. These include elastic and inelastic scattering, and coherent and incoherent scattering. The specific features of these different components will be illustrated using brief examples. We will focus mostly on methods that have already been used for studies of mineral behaviour, and will only briefly comment on methods (such as measurements of magnetic properties, small-angle scattering and surface reflectometry) that have yet to be used for routine studies.

2. General formalism for neutron scattering

2.1 The neutron scattering law

A typical neutron scattering experiment will involve measuring the intensity of the neutrons scattered from a beam incident on a sample. The scattering process will involve a change in the wave vector of the beam, which is denoted by the scattering vector $\mathbf{Q}$. The scattering process may also involve a change in the energy of the neutrons E. This will be determined by the angular frequency ω of some dynamic fluctuation in the sample, so that

$$E = \hbar\omega \qquad (1).$$

The intensity measured in an experiment is converted into a function of $\mathbf{Q}$ and ω, and is proportional to the dynamical structure factor, $S(\mathbf{Q},\omega)$. This function represents the Fourier transforms of the time and spatial fluctuations of the atomic density (or spin density for magnetic neutron scattering). We present the formalism by considering the scattering from point particles, which is appropriate to the case of neutron scattering because, as noted earlier, the length scale of the interaction between a neutron and atomic nucleus is around five orders of magnitude smaller than the wavelength of the neutron beam. For a given particle of label j at position $\mathbf{r}_j$ at time t, the number density can be expressed as the Dirac delta function:

$$\rho_j(\mathbf{r},t) = \delta\big(\mathbf{r} - \mathbf{r}_j(t)\big) \qquad (2).$$

The spatial Fourier transform of the number density is given as

$$\rho_j(\mathbf{Q},t) = \int \rho_j(r,t)\exp(i\mathbf{Q}\cdot\mathbf{r})\mathrm{d}\mathbf{r} = \exp(i\mathbf{Q}\cdot\mathbf{r}_j(t)) \qquad (3).$$

The fluctuations in time are expressed through the cross-correlation function

$$f_{jk}(\mathbf{Q},t) = \langle \rho_j(\mathbf{Q},t)\rho_k(-\mathbf{Q},0)\rangle \quad (4),$$

where the angular brackets denote an average over all initial times. In a neutron scattering process, the contribution of each atomic nucleus to the amplitude of the scattered beam is weighted by the scattering length b_j, which reflects the strength of the interaction between the neutron and the nucleus. As a result, when we consider the fluctuations of the whole sample that will give rise to the neutron scattering, we weight each contribution accordingly and write

$$\begin{aligned} F(\mathbf{Q},t) &= \frac{1}{N}\sum_{j,k}\langle b_j b_k \rho_j(\mathbf{Q},t)\rho_k(-\mathbf{Q},0)\rangle \\ &= \frac{1}{N}\sum_{j,k}\overline{b_j b_k}\langle \rho_j(\mathbf{Q},t)\rho_k(-\mathbf{Q},0)\rangle \end{aligned} \quad (5),$$

where N is the number of atoms. This function is known as the *intermediate scattering function*. The overbars represent the average implicit in the time averaging of the cross-correlation functions, and can be separated from the fluctuations in the density functions because the scattering lengths do not depend on time.

The dynamical structure factor is given by the time Fourier transform of $F(\mathbf{Q},t)$:

$$\begin{aligned} S(\mathbf{Q},\omega) &= \int F(\mathbf{Q},t)\exp(i\omega t)\mathrm{d}t \\ &= \frac{1}{N}\int\sum_{j,k}\overline{b_j b_k}\langle \rho_j(\mathbf{Q},t)\rho_k(-\mathbf{Q},0)\rangle\exp(i\omega t)\mathrm{d}t \end{aligned} \quad (6).$$

In many cases this is expressed in terms of energy rather than angular frequency, using the conversion given in equation (1):

$$S(\mathbf{Q},E) = \frac{1}{N}\int\sum_{j,k}\overline{b_j b_k}\langle \rho_j(\mathbf{Q},t)\rho_k(-\mathbf{Q},0)\rangle\exp(iEt/\hbar)\mathrm{d}t \quad (7).$$

The formalism may now appear to be rather complicated, but we can turn this to our advantage by considering special cases, each of which leads to a special technique that can give more-or-less unique information about the system being studied. This includes separation of coherent from incoherent scattering processes, elastic from inelastic scattering processes (both of which are discussed immediately below), and techniques in which we can integrate over either energy or scattering vector. It is the fact of being able to carry out the separation of different scattering processes that leads to the versatility of neutron scattering methods highlighted in the introduction.

2.2 Separation of coherent and incoherent neutron scattering

In discussions of $S(\mathbf{Q},\omega)$, it is often assumed that the neutron scattering length for any element in a crystal is the same for each atom of a particular element. This implies the assumption that the scattering length is independent of the nuclear isotope number and the nuclear spin state. In practice, what we have actually been doing is to average out all these effects, as we will see below.

For many nuclei, the spin is zero so that the spin-dependent components of the nucleus–neutron interactions are absent, and even when the nuclei have spin, the spin effects are often relatively weak. Moreover, for many important elements only one isotope occurs in significant quantities. For example, the isotopes of oxygen, ^{15}O, ^{16}O and ^{17}O, occur with relative abundances 1%, 98% and 1% respectively. Hence the assumption of constant scattering length for the atoms of many elements is quite justified. However, there are important exceptions. The two major isotopes of nickel are ^{58}Ni (relative abundance of 68.3%) and ^{60}Ni (relative abundance of 26.1%), with respective scattering lengths of 14.4 and 2.8 fm, with neither of these two nuclei having a non-zero value of the spin. On the other hand, hydrogen (^{1}H) is an example where the spin-dependence of the nucleus–neutron (in this case the proton–neutron) interaction is very important, and this isotope has a relative abundance of more than 99.9% in natural hydrogen. The proton and neutron both have spin values of 1/2, which under the laws of quantum mechanics can be aligned in four ways. Three of these have parallel alignment, giving a total spin of $S = 1$ and z component $S_z = -1$, 0 or +1, whereas the fourth has antiparallel alignment and $S = 0$. The scattering lengths for parallel and antiparallel alignment are 10.4 and –47.4 fm respectively, giving an average value of only –3.74 fm. Sodium is another nucleus with an incoherent scattering cross section that arises from the spin states; the incoherent scattering length, 3.56 fm, is close to the coherent scattering length, 3.63 fm. Vanadium is unusual in that the sum of the coherent contributions is almost zero, with only a significant incoherent cross section. We therefore need to consider how the neutron scattering function can be modified to account for these effects, and we shall find that there are considerable applications from this extended approach. The comparisons between values of the coherent and incoherent scattering cross sections are illustrated in Fig. 1. A compilation of scattering lengths and cross sections has been reproduced by Bée (1988).

In order to account for different scattering lengths for atoms of the same type, we separate the intermediate scattering factor (equation 5) into two components:

$$F(\mathbf{Q},t) = F_{\mathrm{coh}}(\mathbf{Q},t) + F_{\mathrm{inc}}(\mathbf{Q},t) \quad (8).$$

where the *coherent* term is given as

$$F_{\mathrm{coh}}(\mathbf{Q},t) = \frac{1}{N}\int\sum_{j,k}\overline{b}_j\overline{b}_k\langle \rho_j(\mathbf{Q},t)\rho_k(-\mathbf{Q},0)\rangle \quad (9),$$

and the *incoherent* term is given as

$$F_{\mathrm{inc}}(\mathbf{Q},t) = \frac{1}{N}\sum_{j,k}(\overline{b_j b_k} - \overline{b}_j\overline{b}_k)\langle \rho_j(\mathbf{Q},t)\rho_k(-\mathbf{Q},0)\rangle \quad (10).$$

The coherent term has an average value for the scattering length and therefore contains the information about coherent (*i.e.* correlated) processes, such as Bragg and phonon scattering. For most applications, the coherent term is expanded in terms of instantaneous atomic displacements from mean positions, and this enables the formalism to be applied to studies of phonon dispersion curves and

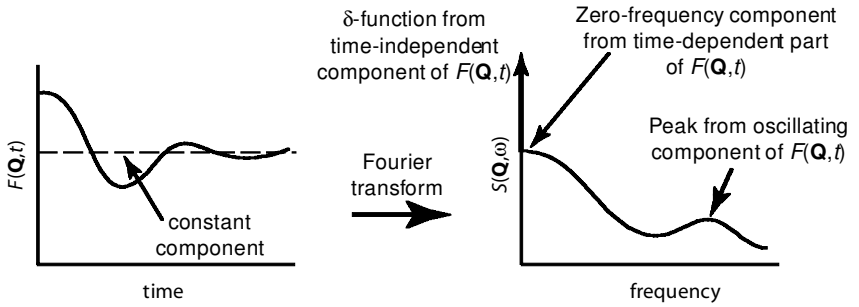

Fig. 2. Illustration of the definition of elastic scattering. The scattering function, $S(\mathbf{Q},\omega)$, is the Fourier transform of a time-correlation function, $F(\mathbf{Q},t)$. If $F(\mathbf{Q},t)$ does not decay to zero value in the long time limit, its Fourier transform will contain a delta function at zero frequency. It is this delta function, and not simply the scattering at zero frequency, that corresponds to elastic scattering.

other dynamic processes. This expansion will be discussed later.

The incoherent term is not yet written in a useful form. We note, however, that we do not expect there to be any correlation between the particular value of the neutron scattering length and the site. This means that we have the condition

$$\overline{b_j b_k} = \overline{b}_j \overline{b}_k \text{ for } j \neq k \qquad (11).$$

Hence only the terms for $j = k$ remain, so that

$$F_{\text{inc}}(\mathbf{Q},t) = \frac{1}{N}\sum_j \left(\overline{b_j^2} - \overline{b}_j^{\,2}\right)\langle \rho_j(\mathbf{Q},t)\rho_j(-\mathbf{Q},0)\rangle \qquad (12).$$

For reference, we can now define two scattering cross sections:

$$\sigma_j^{\text{coh}} = 4\pi \overline{b}_j^{\,2}$$
$$\sigma_j^{\text{inc}} = 4\pi\left(\overline{b_j^2} - \overline{b}_j^{\,2}\right) \qquad (13).$$

We can write the equation for the incoherent structure factor in its expanded form:

$$F_{\text{inc}}(\mathbf{Q},t) = \frac{1}{4\pi N}\sum_j \sigma_j^{\text{inc}} \langle \exp(i\mathbf{Q}\cdot[\mathbf{r}_j(t) - \mathbf{r}_j(0)])\rangle \qquad (14).$$

It is convenient to define a probability distribution function, $G(\mathbf{r}(t),\mathbf{r}(0))$, which gives the probability of finding a particle at a position $\mathbf{r}(t)$ at time t if it had a position $\mathbf{r}(0)$ at time 0. Thus we can write the equation in a new form:

$$F_{\text{inc}}(\mathbf{Q},t) = \frac{1}{4\pi N}\sum_j \sigma_j^{\text{inc}} \int \exp\left(i\mathbf{Q}\cdot[\mathbf{r}_j(t) - \mathbf{r}_j(0)]\right) G(\mathbf{r}(t),\mathbf{r}(0))p(\mathbf{r})\mathrm{d}\mathbf{r}(t)\mathrm{d}\mathbf{r}(0) \qquad (15),$$

where $p(\mathbf{r})$ is the probability of finding the atom at position $\mathbf{r}$ at time 0. The significance of writing the intermediate scattering function this way is that for all problems of interest the time-dependence of the atomic motions are most conveniently analysed through the rate equations that govern the time-dependence of $G(\mathbf{r}(t),\mathbf{r}(0))$.

The main point that should be appreciated at this stage is that the incoherent scattering function contains the dynamic information for individual atoms, provided they have sufficiently large incoherent cross sections. This dynamic information may include the motions due to all the phonon modes in the crystal, complementary to the temperature factor, but it may also include diffusion dynamics if important. This is reviewed briefly below (§4); a comprehensive treatment has been given by Bée (1988).

2.3 Separation of elastic and inelastic scattering

Elastic scattering arises from the static component of a crystal structure (the idea applies equally well to a glass, but not to a fluid phase), and therefore has $\omega = 0$. However, it is not identical with $S(\mathbf{Q},\omega = 0)$, as will now be explained.

The function $S(\mathbf{Q},\omega = 0)$ can be written as

$$S(\mathbf{Q},\omega = 0) = \int F(\mathbf{Q},t)\mathrm{d}t \qquad (16).$$

We can separate $F(\mathbf{Q},t)$ into two components, a constant term and a term that depends on time and either tends to a zero as $t \rightarrow \infty$ or else oscillates around zero at large t. Thus we can write

$$F(\mathbf{Q},t) = F(\mathbf{Q},\infty) + F'(\mathbf{Q},t) \qquad (17),$$

where the first term is the constant term, and the second contains all the time dependence. The Fourier transform of the time-dependent term will give the same energy spectrum for $\omega \neq 0$ as the full $F(\mathbf{Q},t)$. The Fourier transform of the constant term will yield a δ-function at $\omega = 0$:

$$\int F(\mathbf{Q},\infty)\exp(i\omega t)\mathrm{d}t = F(\mathbf{Q},\infty)\delta(\omega) \qquad (18).$$

From equation (5) the function $F(\mathbf{Q},\infty)$ can be written as

$$F(\mathbf{Q},\infty) = \frac{1}{N}\sum_{j,k}\langle b_j b_k \rho_j(\mathbf{Q},\infty)\rho_k(-\mathbf{Q},0)\rangle = \frac{1}{N}\sum_{j,k}\overline{b_j b_k}\langle \rho_j(\mathbf{Q})\rangle\langle \rho_k(-\mathbf{Q})\rangle \qquad (19),$$

where we have used the fact that over infinite times the fluctuations in the density function are uncorrelated. For coherent scattering, equation (9), this will reduce to

$$F_{\text{coh}}(\mathbf{Q},\infty) = \frac{1}{N}\left|\sum_j \overline{b}_j \langle \rho_j(\mathbf{Q})\rangle\right|^2 \qquad (20).$$

The important point to appreciate from this discussion is that the elastic scattering is the Fourier transform of the time-independent component of the intermediate scattering function. The Fourier transform of a constant function will

give a δ-function at zero frequency. This is not the same as the zero-frequency component of the scattered intensity. We illustrate this point in Fig. 2. If $F(\mathbf{Q},t)$ has a relaxational component, the integral of the time-dependent part, which gives a zero-frequency contribution to $S(\mathbf{Q},\omega)$, is non-zero. However, it forms part of the continuous distribution of $S(\mathbf{Q},\omega)$ rather than as a separate δ-function.

2.4 Magnetic neutron scattering

The formalism of neutron scattering can be readily extended for magnetic scattering. To illustrate the point, we consider magnetic diffraction using an unpolarised beam of neutrons. The magnetic equivalent of equation (20) is

$$F_{\mathrm{mag}}(\mathbf{Q},\infty) = \frac{1}{N}\left|\sum_j \mathbf{q}_j p_j \langle \exp(i\mathbf{Q}\cdot\mathbf{r}_j)\rangle\right|^2 \qquad (21),$$

where the *magnetic interaction vector* $\mathbf{q}$ is given by

$$\mathbf{q} = \mathbf{m}/m - \mathbf{Q}(\mathbf{Q}\cdot\mathbf{m})/Q^2 m \qquad (22),$$

and $\mathbf{m}$ is the magnetic moment of an atom or ion. If α is the angle between $\mathbf{m}$ and $\mathbf{q}$,

$$q = |\mathbf{q}| = \sin\alpha \qquad (23).$$

The *magnetic scattering amplitude*, p, is given by

$$p = \frac{e^2\gamma}{2mc^2} gJf \qquad (24),$$

where e is the electron charge, γ is the magnetic moment of the neutron, m is the mass of the electron, and c is the speed of light. g is the Landé factor, J is the total orbital angular momentum number of the atom, and gJ gives the magnetic moment of the atom. f is the form factor that depends on Q in a similar manner to the behaviour of the X-ray atomic scattering factor. Over the useful range of values of Q, p has values similar to the values of the neutron scattering length for nuclear scattering, b (Fig. 1). We will not develop the theory of magnetic scattering in this review, but it should be noted that the formalism for nuclear scattering presented here, both for elastic and inelastic scattering, can be extended for the study of the structures and dynamics of magnetic materials.

3. Formalism for coherent neutron scattering

3.1 Coherent inelastic neutron scattering

We now develop the analysis of the neutron scattering function for the case when atoms vibrate about their mean positions, as in a crystalline solid (for more details, see Ashroft & Mermin, 1976; Dove, 1993). The instantaneous position of atom j can be written as

$$\mathbf{r}_j(t) = \mathbf{R}_j + \mathbf{u}_j(t) \qquad (25)$$

where $\mathbf{R}_j$ is the average position of the atom, and $\mathbf{u}_j(t)$ represent the instantaneous displacement of the atom from its average position. The intermediate scattering function, equation (9), can therefore be written as

$$F(\mathbf{Q},t) = \frac{1}{N}\sum_{j,k}\overline{b}_j\overline{b}_k \exp\left(i\mathbf{Q}\cdot[\mathbf{R}_j - \mathbf{R}_k]\right)\langle\exp(i\mathbf{Q}\cdot[\mathbf{u}_j(t) - \mathbf{u}_k(0)])\rangle \qquad (26).$$

If the atoms move with harmonic motions, a standard result gives

$$\left\langle\exp\left(i\mathbf{Q}\cdot[\mathbf{u}_j(t) - \mathbf{u}_k(0)]\right)\right\rangle = \exp\left(-\frac{1}{2}\langle(\mathbf{Q}\cdot[\mathbf{u}_j(t) - \mathrm{u}_k(0)])^2\rangle\right)$$

$$= \exp\left(-\frac{1}{2}\langle[\mathbf{Q}\cdot\mathbf{u}_j(t)]^2\rangle - \frac{1}{2}\langle[\mathbf{Q}\cdot\mathbf{u}_k(0)]^2\rangle + \langle[\mathbf{Q}\cdot\mathbf{u}_j(t)][\mathbf{Q}\cdot\mathbf{u}_k(0)]\rangle\right) \qquad (27).$$

The first two terms in the expanded exponent correspond to the normal temperature factors (see Willis & Pryor, 1975; Ashcroft & Mermin, 1976; Castellano & Main, 1985):

$$\exp\left(-\frac{1}{2}\langle[\mathbf{Q}\cdot\mathbf{u}_j(t)]^2\rangle\right) = \exp(-W_j)\ ;$$

$$\exp\left(-\frac{1}{2}\langle[\mathbf{Q}\cdot\mathbf{u}_k(0)]^2\rangle\right) = \exp(-W_k) \qquad (28).$$

The third term can be expanded as a power series:

$$\exp\left(\langle[\mathbf{Q}\cdot\mathbf{u}_j(t)][\mathbf{Q}\cdot\mathbf{u}_k(0)]\rangle\right) = \sum_{m=0}^{\infty}\frac{1}{m!}\langle[\mathbf{Q}\cdot\mathbf{u}_j(t)][\mathbf{Q}\cdot\mathbf{u}_k(0)]\rangle^m \qquad (29).$$

The first term in the series, $m = 0$, corresponds to elastic scattering, which we will discuss below. The second term, $m = 1$, turns out to be the most interesting of the other terms in the series. Within the harmonic theory of lattice dynamics, the instantaneous displacement can be written as

$$\mathbf{u}_j(t) = \frac{1}{(Nm_j)^{1/2}}\sum_{\mathbf{k},\nu}\mathbf{e}_j(\mathbf{k},\nu)\exp(i\mathbf{k}\cdot\mathbf{r}_j)Q(\mathbf{k},\nu) \qquad (30),$$

where $Q(\mathbf{k},\nu)$ is the normal mode coordinate for a phonon of wave vector $\mathbf{k}$ and branch ν (the number of branches in a crystal containing z atoms per unit cell is equal to $3z$), and $\mathbf{e}_j(\mathbf{k},\nu)$ is the normalised vector that gives the relative displacements of each atom. Treating the normal mode coordinate as a quantum operator, it can be shown that the $m = 1$ term contributes the following term to the dynamical scattering factor:

$$S_1(\mathbf{Q},\omega) = \frac{1}{N}\sum_{j,k}\overline{b}_j\overline{b}_k \exp\left(i\mathbf{Q}\cdot[\mathbf{R}_j - \mathbf{R}_k]\right)\exp(-W_j - W_k)$$

$$\int\langle[\mathbf{Q}\cdot\mathbf{u}_j(t)][\mathbf{Q}\cdot\mathbf{u}_k(0)]\rangle\exp(-i\omega t)\mathrm{d}t$$

$$= \frac{1}{N}\sum_{\nu}\frac{\hbar}{2\omega(\mathbf{k},\nu)}\left|F_\nu(\mathbf{Q})\right|^2$$

$$\left([1 + n(\omega)]\delta(\omega + \omega(\mathbf{k},\nu)) + n(\omega)\delta(\omega - \omega(\mathbf{k},\nu))\right) \qquad (31),$$

where the phonon structure factor component is given as

$$F_\nu(\mathbf{Q}) = \sum_j \frac{\overline{b}_j}{m_j}\exp(-W_j)\exp(i\mathbf{Q}\cdot\mathbf{R}_j)\mathbf{Q}\cdot\mathbf{e}(\mathbf{k},\nu) \qquad (32).$$

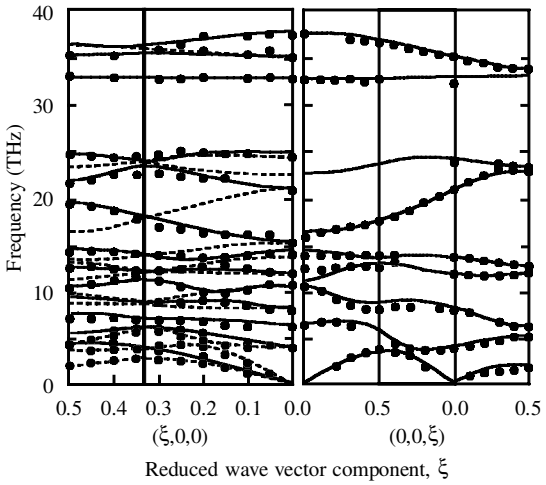

Fig. 3. Phonon dispersion curves of quartz obtained by inelastic neutron scattering measurements, using a triple-axis spectrometer at the ILL reactor neutron source (Strauch & Dorner, 1993).

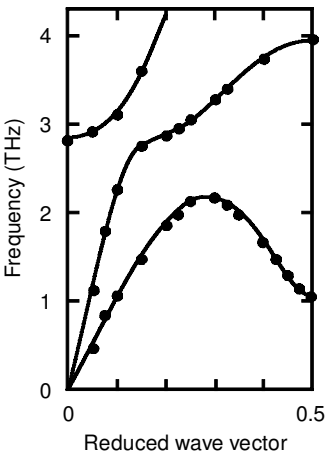

Fig. 4. Phonon dispersion curves for calcite along the direction (000) to (1/2,0,–2) in reciprocal space, measured using a triple-axis spectrometer at the Chalk River reactor neutron source. The important point is the dip in the lowest-frequency branch at the zone boundary wave vector (Dove *et al.*, 1992).

The formula for the one-phonon dynamical scattering factor requires some unpacking. The Dirac delta functions represent the fact that scattering from a phonon of angular frequency $\omega(\mathbf{k},\nu)$ only occurs for changes in the energy of the neutron beam of $\pm\hbar\omega(\mathbf{k},\nu)$. The probability of phonon scattering is determined by the thermal population of phonons, which is determined by the Bose-Einstein factor $n(\omega)$:

$$n(\omega) = \frac{1}{\exp(\hbar\omega/k_{\mathrm{B}}T)-1} \qquad (33).$$

The case where the scattering mean has lost energy corresponds to the situation where the neutron beam has scattered following the creation of a phonon, and this process occurs with probability $[1 + n(\omega)]$. The case where the scattered beam gains energy corresponds to the situation where the neutron beam absorbs a phonon, and probability of this process is given by the number of phonons $n(\omega)$. At high temperatures the intensity from a single phonon is proportional to

$$S_1(\mathbf{Q},\omega) \propto \frac{k_{\mathrm{B}}T}{\omega^2}\ \delta(\omega \pm \omega(\mathbf{k},\nu)) \qquad (34).$$

In both cases the intensity of scattering is determined by the phonon structure factor which accounts for the relative positions of atoms and the relative orientations of the scattering vector $\mathbf{Q}$ and the displacements of the atoms. These factors give selection rules for the one-phonon neutron scattering process, which are not as restrictive as the selection rules in Raman or infrared spectroscopy, and which can be useful in separating measurements when there are a large number of phonons for any wave vector $\mathbf{k}$.

The terms for $m > 1$ involve *multiphonon* processes. These processes do not give enough structure in measured spectra to be useful, and understanding the behaviour of these processes is mostly motivated by the need to subtract them from absolute measurements of intensities in both inelastic and total scattering measurements.

The one-phonon coherent inelastic processes described above are often used for measurements of phonon dispersion curves with single crystal samples (Chaplot *et al.*, 2002). These studies are not trivial, and as a result it is often the case that measurements will only focus on a small subset of all phonon modes (particularly the lower energy modes). Examples of measurements of relatively complete sets of dispersion curves of minerals include calcite (Cowley & Pant, 1970), sapphire (Schober *et al.*, 1993) and quartz (Strauch & Dorner, 1993). The measured dispersion curves for quartz are shown in Fig. 3. It should be appreciated that the measurements of the high-frequency modes are particularly difficult – it can be seen from equation (34) that the one-phonon intensity scales as ω^{-2}. Since these modes can be better accessed by other spectroscopic probes, and indeed their variation across range of wave vector is often slight, it is often not worth attempting to measure complete sets of dispersion curves. Moreover, the experimental difficulties are increased with more complex minerals. Examples of partial sets of dispersion curves include the olivines forsterite (Rao *et al.*, 1988) and fayalite (Ghose *et al.*, 1991), pyrope (Artioli *et al.*, 1996b), andalusite (Winkler & Bührer, 1990) and zircon (Mittal *et al.*, 2000a).

Because of the difficulties in obtaining full dispersion curves, inelastic coherent scattering measurements using single crystals may focus on selected modes. An example is a detailed study of an anomalous inelastic scattering process associated with a particular zone boundary mode in calcite (Dove *et al.*, 1992; Harris *et al.*, 1998). The relevant phonon dispersion relation is shown in Fig. 4. The frequency of the lowest mode dips considerably at the zone boundary, and softens on increasing temperature. This is shown in inelastic neutron scattering spectra for different temperatures in Fig. 5. This mode is actually the soft mode for the high-pressure displacive phase transition in calcite. In addition to the phonon peak, there is a broad band of

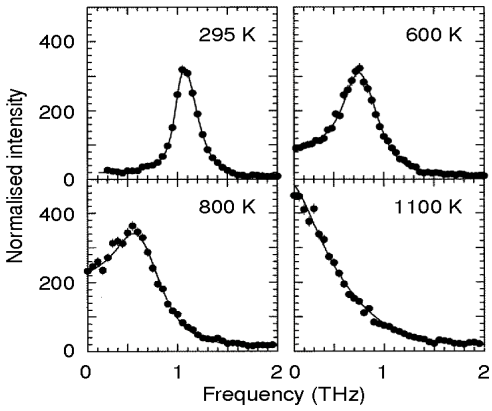

Fig. 5. Inelastic neutron scattering spectra from calcite at the (1/2,0,–2) zone boundary point for several temperatures. The important points are the phonon peak that softens on heating, and the additional scattering at lower frequencies that increases dramatically on heating (Harris *et al.*, 1998).

inelastic scattering that is localised (in Q) at the zone boundary. This anomalous inelastic scattering can be seen as a weak feature barely above the background level at energies lower than the phonon peak at ambient temperature in Fig. 5. The intensity of this scattering increases rapidly on heating, eventually dominating the spectra at high temperatures. The spectra have been analysed by using a model in which the phonon is coupled to a relaxation process in the crystal, although there is no clear identification of the nature of this relaxation process. There is an order-disorder phase transition at 1260 K (which has also been studied by neutron powder diffraction, Dove & Powell 1989). Phonon instabilities associated with phase transitions have also been studied by inelastic neutron scattering in quartz (Boysen *et al.*, 1980; Bethke *et al.*, 1987, 1992; Dolino *et al.*, 1992) and leucite (Boysen, 1990).

It is also possible to perform inelastic coherent scattering measurements on polycrystalline samples, either performing measurements as a function of the modulus of the scattering vector, Q, or integrating over all Q to obtain a weighted phonon density of states. The latter type of measurement was used to obtain the first experimental evidence for a significant enhancement of low-energy rigid-unit modes in the high-temperature phase of cristobalite (Swainson & Dove, 1993). Measured phonon densities of states have been reported for complex minerals such as almandine (Mittal *et al.*, 2000b), pyrope (Pavese *et al.*, 1998), sillimanite and kyanite (Rao *et al.*, 1999), orthoenstatite (Choudhury *et al.*, 1998) and fayalite (Price *et al.*, 1991).

With spectrometers such as the MARI instrument at ISIS it is now possible to perform inelastic scattering measurements from powdered samples as functions of Q. The value of these types of measurements is that they enable comparisons to be made between the excitation spectra of different phases. Fig. 6 shows measurements for the two phases of cristobalite (Dove *et al.*, 2000a). It is clear that there is considerable additional scattering at low energies (below 5 meV) in the high-temperature disordered phase. This scattering can be associated with the rigid-unit modes discussed by Swainson & Dove (1993), Hammonds *et al.* (1996) and Dove *et al.* (2000b and c). It has also been shown by these measurements that the inelastic neutron scattering spectra of silica glass is closely related to the spectra of the two phases of cristobalite (Dove *et al.*, 2000a and b).

There has been a considerable effort in the physics and chemistry communities to use inelastic neutron scattering methods to study magnetic dynamics, which can often be described as *spin waves*. Measurements of spin wave dispersion curves can provide information about the interactions between atomic magnetic moments, the so-called *exchange interactions*. There have been comparatively few inelastic neutron scattering measurements on magnetic minerals. Spin wave dispersion curves have been reported for hematite (Samuelson & Shirane, 1970), and crystal field magnetic transitions in Co-bearing cordierite and spinel phases have been studied by inelastic neutron scattering (Winkler *et al.*, 1997).

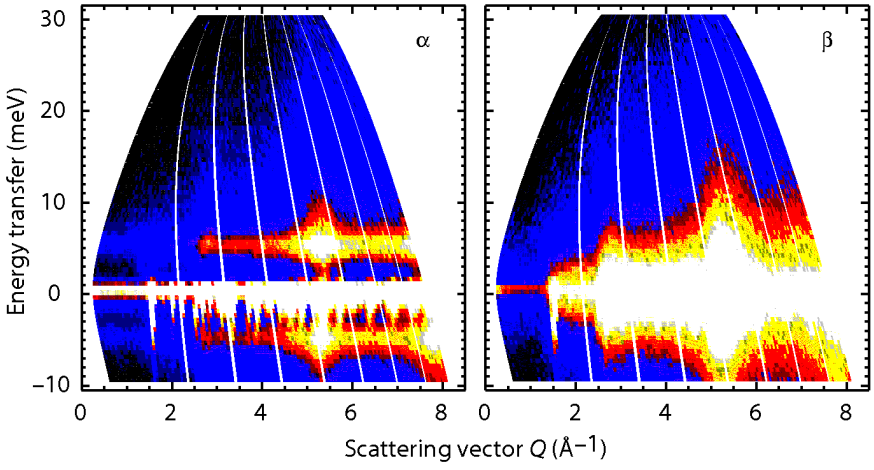

Fig. 6. Inelastic neutron scattering data for the two phases of cristobalite, obtained as functions of both scattering vector and energy transfer. High intensities are shown as lighter shading. The important point of comparison is the additional scattering seen at low energies in the high-temperature β phase. The data were obtained on the MARI chopper spectrometer at the ISIS spallation neutron source.

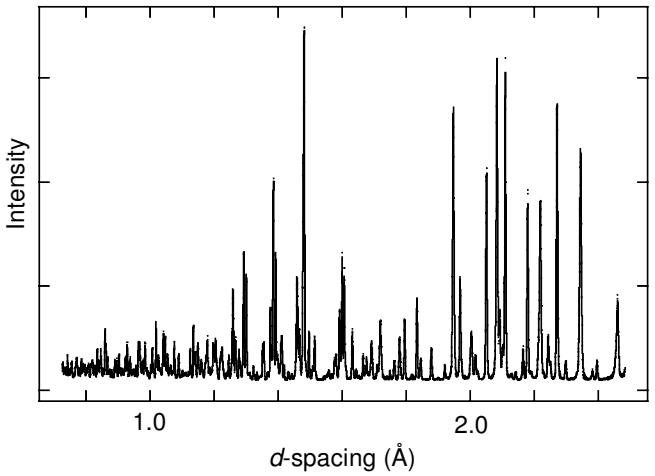

Fig. 7. High-resolution powder diffraction measurement from orthoenstatite, obtained on the HRPD diffractometer at the ISIS spallation neutron source (courtesy of S.A.T Redfern).

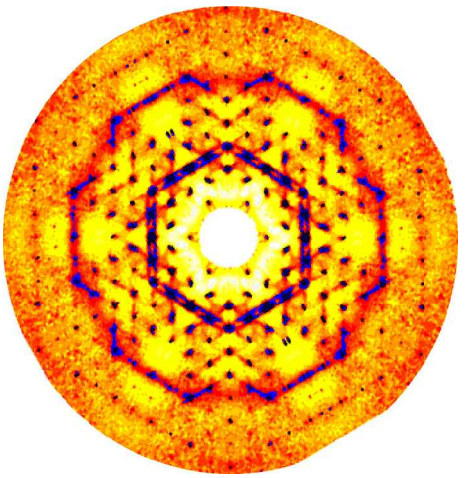

Fig. 8. Map of diffuse scattering measured in β-quartz, using the PRISMA indirect-geometry spectrometer at the ISIS spallation neutron source (Tucker *et al.*, 2001a). The most intense scattering is shown as the darker regions (such as the scattering from the points in the reciprocal lattice). The most important features are the streaks of diffuse scattering, which correspond to low-energy rigid unit phonon modes (Hammonds *et al.*, 1996).

3.2 Coherent elastic scattering and Bragg scattering

The case $m = 0$ in equation (29) gives the result:

$$F_0(\mathbf{Q},t) = \frac{1}{N}\sum_{j,k}\overline{b}_j\overline{b}_k \exp\left(i\mathbf{Q}\cdot[\mathbf{R}_j - \mathbf{R}_k]\right)\exp(-W_j - W_k)$$
$$= \frac{1}{N}\left|\sum_j \overline{b}_j \exp(i\mathbf{Q}\cdot\mathbf{R}_j)\exp(-W_j)\right|^2 \quad (35).$$

This result is independent of time. As a result, the time Fourier transform gives a delta function:

$$S_0(Q,\omega) = \int F_0(\mathbf{Q},t)\exp(-i\omega t)\mathrm{d}t$$
$$= \frac{1}{N}\left|\sum_j \overline{b}_j \exp(i\mathbf{Q}\cdot\mathbf{R}_j)\exp(-W_j)\right|^2 \delta(\omega) \quad (36).$$

This result is equivalent to the elastic scattering, *i.e.* the $\omega = 0$ limit of $S(\mathbf{Q},\omega)$, obtained earlier, equations (18) and (19). This can be demonstrated by starting from the general equation for the intermediate structure factor for coherent neutron scattering:

$$\sum_j \overline{b}_j \langle\exp(i\mathbf{Q}\cdot\mathbf{R}_j)\rangle = \sum_j \overline{b}_j \exp(i\mathbf{Q}\cdot\mathbf{R}_j)\langle\exp(i\mathbf{Q}\cdot\mathbf{u}_j)\rangle$$
$$= \sum_j \overline{b}_j \exp(i\mathbf{Q}\cdot\mathbf{R}_j)\exp(-\langle[\mathbf{Q}\cdot\mathbf{u}_j]^2\rangle) \quad (37).$$

This is the normal Bragg diffraction structure factor, but can be generalised to include glasses. For glasses, its application relies on the fact that the atoms vibrate around mean positions that do not change over the time scale of a measurement. This is not the case for fluids, and as a result there is no elastic scattering for a liquid.

Bragg diffraction is commonly used in two modes. The most common is powder diffraction, with data analysed using the Rietveld refinement method. This method is now quite fast on a high-intensity neutron source, and resolution can also be high. An example of a high-resolution measurement is shown in Fig. 7. Powder diffraction can be used for studying the response of a structure to changes in temperature or pressure, particularly if there is a displacive or order/disorder phase transition. Examples of temperature-induced displacive phase transitions studied by neutron powder diffraction include cristobalite (Schmahl *et al.*, 1992), leucite (Palmer *et al.*, 1997), calcite and the analogue sodium nitrate (Swainson *et al.*, 1997) and lawsonite (Myer *et al.*, 2001). Examples of the use of neutron powder diffraction for the study of cation ordering include the åkermanite–gehlenite solid solution (Swainson *et al.*, 1992), Mn/Mg ordering in cummingtonite (Reece *et al.*, 2000) and cation ordering in other amphiboles (Welch & Knight, 1999), cation ordering in the ilmenite–hematite solid solution (Harrison *et al.*, 2000), cation ordering in various spinel phases and spinel solid solutions (Harrison *et al.*, 1998, 1999; Pavese *et al.*, 1999a,b and 2000a; Redfern *et al.*, 1999), and cation partioning in olivine phases (Henderson *et al.*, 1996; Redfern *et al.*, 1998, 2000), and phengite (Pavese *et al.*, 1997, 1999c, 2000b). Powder diffraction is an excellent tool for the variation of structure with temperature for properties such as thermal expansion, *e.g.* crocoite (Knight, 2000), or for studies of dehydration, *e.g.*, gypsum (Schofield *et al.*, 1997) and fluorapophyllite (Stahl *et al.*, 1987). As noted in §1.2, neutron scattering is much more sensitive to scattering from hydrogen or deuterium than X-rays, and because of this neutron powder diffraction has often been used to study the behaviour of hydrogen in minerals. Examples include analcime (Line *et al.*, 1996), laumontite (Stahl & Artioli, 1993), lawsonite (Myer *et al.*, 2001), gypsum (Schofield *et al.*, 2000) and the amphiboles (Welch & Knight, 1999; Reece *et al.*, 2000). Recent exciting developments in high-pressure neutron scattering are most advanced in powder diffraction. Examples of some of the studies that have been carried out include several studies of brucite (Parise *et al.*, 1993; Catti *et al.*, 1995; Le Godec *et al.*, 2001, 2002), FeSi (Wood *et al.*, 1997), hydrogarnet (Lager & von Dreele, 1996), cristobalite (Dove *et al.*, 2000), muscovite (Catti *et al.*, 1994) and Phase A (Kagi *et al.*,

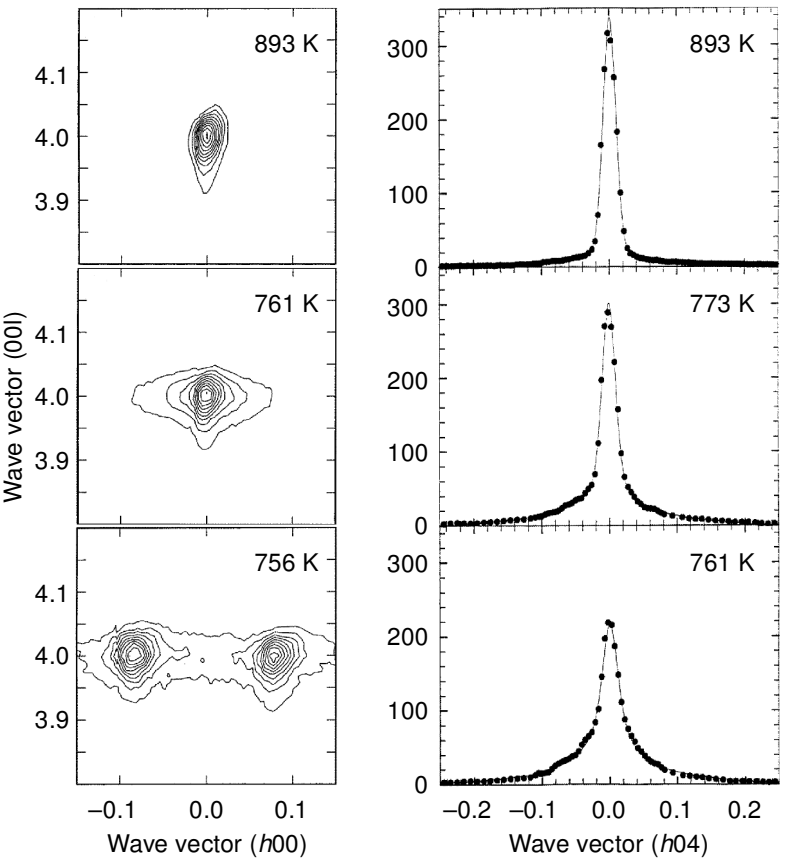

Fig. 9. *Left*: maps of scattering from Na_2CO_3 at various temperatures, showing the Bragg peaks and the diffuse scattering associated with the Bragg peaks. *Right*: cuts through the Bragg peaks, showing the decline of the intensity in the Bragg peaks on cooling towards the phase transition and the growth of diffuse scattering around the Bragg peaks. The data have been fitted by a model of this type of ferroelastic phase transition. The measurements were obtained by Harris *et al.* (1996) on the PRISMA indirect-geometry spectrometer at the ISIS spallation neutron source.

2000). It is now possible to perform neutron powder diffraction meaurements at simultaneous high pressures and temperatures (Zhao *et al.*, 1999, 2000; Le Godec *et al.*, 2001, 2002).

Neutron Bragg diffraction can also be used with single crystals (Artioli, 2002). Single-crystal diffraction is capable of giving structural information with higher precision than with powder diffraction, although at the cost of a greatly increased time necessary for a single measurement that precludes studies at many temperatures or pressures. Examples of single-crystal neutron diffraction measurements include anorthite (Ghose *et al.*, 1993), beryl (Artioli *et al.*, 1995a), pyrope (Artioli *et al.*, 1997), diopside (Prencipe *et al.*, 2000), enstatite (Ghose *et al.*, 1986), cation ordering in olivine (Artioli *et al.*, 1995b; Rinaldi *et al.*, 2000) and hydrogen bonding in schultenite (Wilson, 1994).

In addition to the use of Bragg diffraction for determination and refinement of crystal structures, Bragg diffraction can be used to give information about the internal states of stress within a material. This is reviewed by Schäfer (2002). A few magnetic neutron diffraction measurements have been reported. These include ilvaite (Ghose *et al.*, 1984, 1990), hedenbergite (Coey & Ghose, 1985), Li-aegerine (Redhammer *et al.*, 2001) and the ilmenite-hematite solid solution (Harrison & Redfern, 2001).

3.3 Coherent diffuse scattering

The coherent diffuse scattering from a crystalline material is defined as the total diffraction with the Bragg scattering subtracted. The diffuse scattering corresponds to a measurement of $S(\mathbf{Q},\omega)$ at a fixed value of $\mathbf{Q}$ integrated over all ω:

$$S(\mathbf{Q}) = \int S(\mathbf{Q},\omega)\mathrm{d}\omega \qquad (38).$$

Since $F(\mathbf{Q},t)$ is the reverse Fourier transform of $S(\mathbf{Q},\omega)$, the equation for $S(\mathbf{Q})$ is simply the zero-time component of the reverse Fourier transform:

$$S(\mathbf{Q}) = F(\mathbf{Q},0) = \frac{1}{N}\sum_{j,k}\overline{b}_j\overline{b}_k\langle\exp(i\mathbf{Q}\cdot\mathbf{r}_j)\exp(-i\mathbf{Q}\cdot\mathbf{r}_k)\rangle \qquad (39).$$

Expressing this in terms of the density functions, and subtracting the Bragg scattering to give the diffuse scattering, we obtain

$$S_{\mathrm{diffuse}}(\mathbf{Q}) = \frac{1}{N}\sum_{j,k}\overline{b}_j\overline{b}_k\left(\langle\rho_j(\mathbf{Q})\rho_k(-\mathbf{Q})\rangle - \langle\rho_j(\mathbf{Q})\rangle\langle\rho_k(-\mathbf{Q})\rangle\right) \qquad (40).$$

The diffuse scattering can therefore be seen as arising from instantaneous fluctuations of the atomic density from the average density. Many aspects of the technique of neutron diffuse scattering have recently been discussed by Nield & Keen (2001).

There have been far fewer studies of minerals using diffuse scattering than diffraction studies. An example of a measurement of diffuse scattering from a single crystal of quartz heating into the high-temperature β phase is shown in Fig. 8 (Tucker *et al.*, 2001a). The important features are the streaks of diffuse scattering, which correspond to scat-

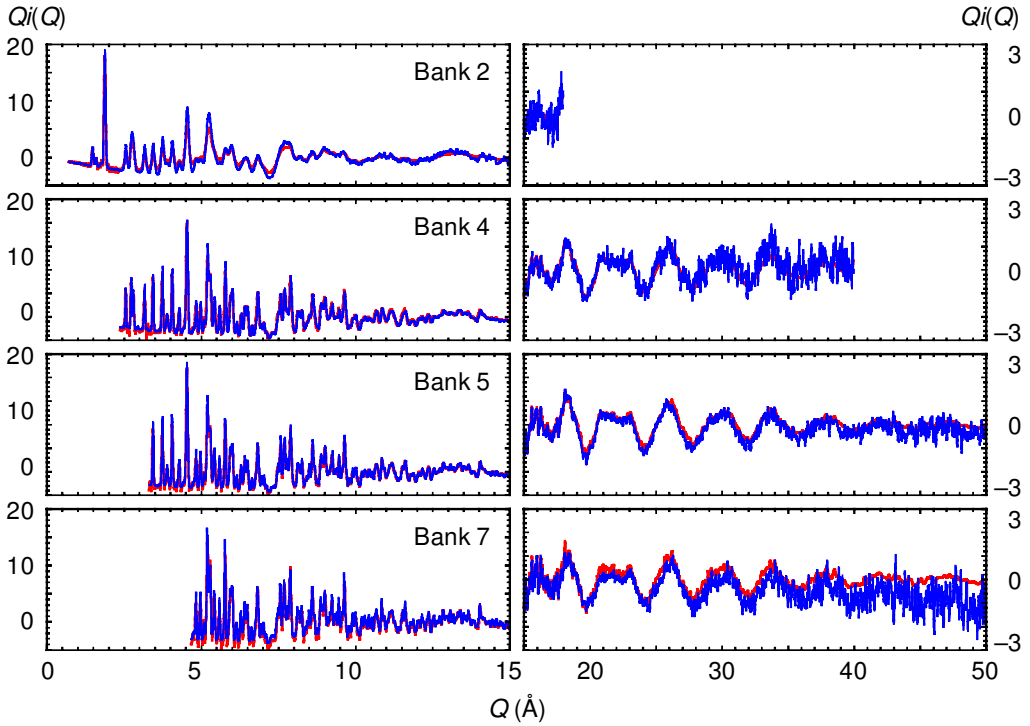

Fig. 10. Total scattering data, $Qi(Q)$, for a polycrystalline sample of berlinite at ambient temperature, with data from different banks of detectors being shown separately. The curves through the data are fits using an inverse Monte Carlo method (Tucker *et al.*, 2002). The data were obtained on the GEM diffractometer at the ISIS spallation neutron source.

tering from low-frequency rigid unit phonon modes (Hammonds *et al.*, 1996), and which are less prominent in diffuse scattering measurements from the α phase. The main problem with such large-scale diffuse scattering measurements lies in the interpretation. It is very difficult to develop data-based models, and such measurements are usually used for comparing with independent model calculations.

Diffuse scattering measurements have more success for the study of specific features as a function of temperature, such as critical scattering associated with a phase transition. An example is the study of the critical scattering associated with the phase transition in $NaNO_3$ (Payne *et al.*, 1997). An interesting example is the diffuse scattering in Na_2CO_3 associated with the displacive hexagonal–monoclinic phase transition at 760 K (Harris *et al.*, 1996); a neutron powder diffraction study of the phase transition has been reported by Harris *et al.* (1993) and Swainson *et al.* (1995). Maps of the single-crystal diffuse scattering are shown for several temperatures in Fig. 9, together with detailed cuts through the peaks of diffuse scattering. This phase transition is an unusual example of a second-order ferroelastic phase transition in which the acoustic softening takes place over a plane of wave vectors (the acoustic softening is seen macroscopically as the softening of the c_{44} elastic constant, which is isotropic within the plane normal to [001]). It has been shown on general grounds that the ferroelastic instability in such as case will lead to a divergence of the temperature factors, similar to the behaviour in two-dimensional melting (Mayer & Cowley, 1988). This will lead to the Bragg peaks vanishing, being replaced by broad diffuse scattering. This effect is clearly seen in the data shown in Fig. 9.

3.4 Coherent total scattering

When dealing with isotropic samples, we have to average the scattering function over all relative orientations of **Q** and **r**. We write $r_{jk} = |\mathbf{r}_j - \mathbf{r}_k|$, and obtain the orientational average ($Q = |\mathbf{Q}|$):

$$\begin{aligned}\langle \exp(i\mathbf{Q}\cdot[\mathbf{r}_j - \mathbf{r}_k])\rangle &= \frac{1}{4\pi}\int_0^{2\pi} \mathrm{d}\varphi \int_0^{\pi} \sin\theta \mathrm{d}\theta \exp(iQr_{jk}\cos\theta) \\ &= \frac{1}{2}\int_{-1}^{+1} \exp(iQr_{jk}x)\mathrm{d}x \\ &= \frac{\sin(Qr_{jk})}{Qr_{jk}} \end{aligned} \quad (41).$$

Using this average, we obtain

$$\begin{aligned} S(Q) &= \frac{1}{N}\sum_{j,k} \overline{b}_j \overline{b}_k \sin(Qr_{jk})/Qr_{jk} \\ &= \frac{1}{N}\sum_j \overline{b}_j^2 + \frac{1}{N}\sum_{j\neq k} \overline{b}_j \overline{b}_k \sin(Qr_{jk})/Qr_{jk} \end{aligned} \quad (42),$$

where we separate the terms involving the same atoms (the *self terms*) and those involving interference between different atoms.

Rather than perform a summation over all atoms pairs, we can express the equation using pair distribution functions. First we define $g_{mn}(r)\mathrm{d}r$ as the probability of finding a pair of atoms of types m and n with separation between r and $r + \mathrm{d}r$. This function will have peaks corresponding to specific sets of interatomic distances. For example, in silica (SiO_2) there will be a peak corresponding to the Si–O bond at ~1.6 Å, a peak corresponding to the O–O bond at ~2.3 Å, and a third peak corresponding to the nearest-neighbour Si…Si distance at ~3.2 Å. $g(r)$ will be zero for all r below the shortest interatomic distance, and

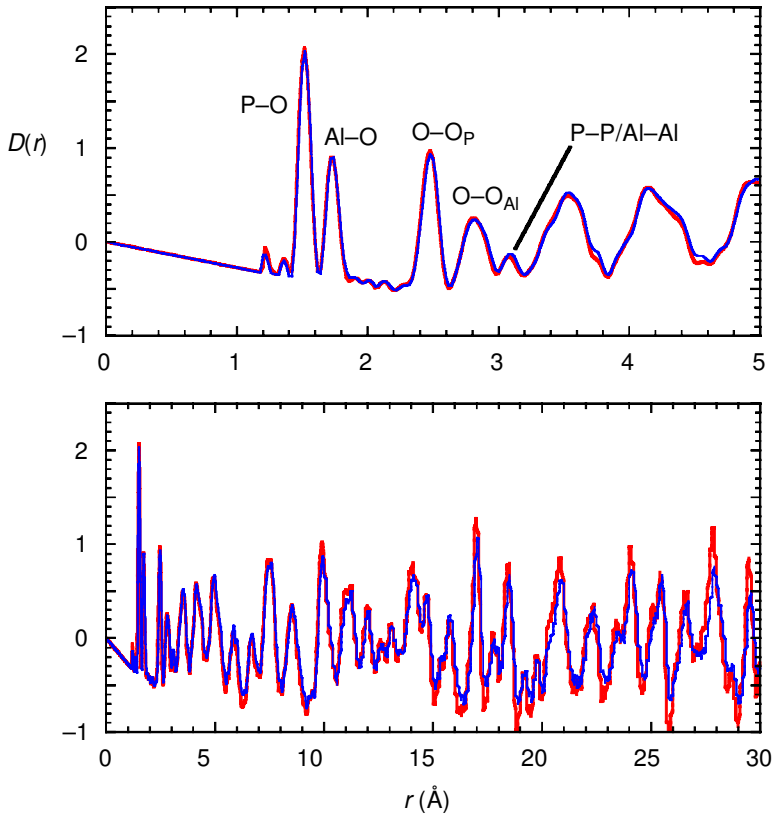

Fig. 11. The $D(r)$ pair distribution function for berlinite, obtained as the Fourier transform of the total scattering data show in Fig. 10 using an inverse transform method (Tucker *et al.*, 2002). The features in $D(r)$ are associated with interatomic distances. The resolution on the measurement is good enough to differentiate between the interatomic distances associated with the AlO_4 and PO_4 tetrahedra.

will tend to a value of 1 at large r. Thus we can rewrite $S(Q)$ as

$$S(Q) = \sum_m c_m \overline{b_m^2} + i(Q) + S_0 \quad (43),$$

$$i(Q) = \rho_0 \sum_{m,n} c_m c_n \overline{b}_m \overline{b}_n \int_0^\infty 4\pi r^2 (g_{mn}(r) - 1) \frac{\sin Qr}{Qr} \, dr \quad (44),$$

where c_m and c_n the proportions of atoms of type m and n respectively, and ρ_0 is the number density. S_0 is determined by the average density, and gives scattering only in the experimentally inaccessible limit $Q \rightarrow 0$. It is convenient to write the pair distribution functions in either of two overall forms:

$$G(r) = \sum_{m,n} c_m c_n \overline{b}_m \overline{b}_n \left(g_{mn}(r) - 1\right) = \sum_{i,j=1}^{n} c_i c_j \overline{b}_i \overline{b}_j \left(g_{ij}(r) - 1\right) \quad (45),$$

$$D(r) = 4\pi r \rho_0 G(r) \quad (46).$$

Thus we can write the scattering equations and associated Fourier transforms as

$$i(Q) = \rho_0 \int_0^\infty 4\pi r^2 G(r) \frac{\sin Qr}{Qr} \, dr \quad (47),$$

$$Qi(Q) = \int_0^\infty D(r) \sin Qr \, dr \quad (48),$$

$$G(r) = \frac{1}{(2\pi)^3 \rho_0} \int_0^\infty 4\pi Q^2 i(Q) \frac{\sin Qr}{Qr} \, dQ \quad (49),$$

$$D(r) = \frac{2}{\pi} \int_0^\infty Qi(Q) \sin Qr \, dQ \quad (50).$$

This formalism is discussed in more detail by Keen (2001) and Dove *et al.* (2002).

The technique of total scattering is described in more detail elsewhere in this special collection (Dove *et al.*, 2002) and by Dove & Keen (1999). To illustrate the point, we show total scattering data $Qi(Q)$ for berlinite, $AlPO_4$, in Fig. 10 obtained using several different banks of detectors in the modern instrument GEM at ISIS. Each bank will measure the total scattering signal over a different range of values of Q. The low-Q data show Bragg peaks superimposed on a background of diffuse scattering. The high-Q data show only oscillatory diffuse scattering, which can be related to the shortest interatomic spacings. The resultant pair distribution function $D(r)$ is shown in Fig. 11.

The important point about the data shown in Fig. 11 is that it has been possible to resolve separately the peaks in the pair distribution functions associated with the AlO_4 and PO_4 tetrahedra. To achieve this resolution it is essential to perform total scattering measurements to large values of Q (see the discussion of Dove *et al.*, 2002). This is something that can be achieved using spallation neutron sources such as ISIS.

Neutron total scattering experiments have been used in studies of phase transitions in various silica polymorphs (Dove *et al.*, 1997, 2000b and c; Keen & Dove, 1999; Tucker *et al.*, 2000a, 2001a and b), for a comparison of the structures of crystalline and amorphous silica (Keen & Dove, 1999, 2000), and for a direct determination of the thermal expansion of the Si–O bond (Tucker *et al.*, 2000b). Further examples are given by Dove *et al.* (2002).

3.5 Small-angle coherent scattering

Most of this article focuses on structural features on the atomic scale, but important processes (such as exsolution) have rather longer length scales (of order 10–1000 Å). These produce density fluctuations over a length scale covering many atoms, which lead to interference effects in the scattered neutron beams. Because the length scales are relatively large, the scattering processes occur for small values of Q, and hence they are called small-angle scattering. Typically the signature of small-angle scattering is a peak centred on $Q = 0$, with a width that is related to the characteristic length scale of the long-range density fluctuations. The strength of the small-angle scattering is determined by the contrast between the mean scattering lengths of different regions in the sample. For this reason small-angle scattering in solids is most easily seen for exsolution processes, where the variation in the density across the sample is associated with clustering of different types of atoms (similarly, one important application of small-angle scattering is to study clustering of molecules in solutions).

The simplest analysis of small-angle scattering is through the Guinier formula, which is appropriate for the exsolution of small particles within a matrix. In this limit, the intensity of small angle scattering is

$$I = I_0 \exp(-Q^2 R_g^2/3) \quad (51),$$

where R_g is the radius of gyration of the particles. For spherical particles of radius R,

$$R_g^2 = 3R/5 \quad (52).$$

Other formulations of the small-angle scattering law have been developed for other mechanisms of density fluctuations, including cases that cannot be described as particles within a matrix. At the time of writing, small-angle scattering is a tool that has yet to be routinely exploited within Earth and Mineral Sciences beyond a few cases, including a study of opals by Graetsch & Ibel (1997).

4. Formalism for incoherent scattering

4.1 General considerations

Hydrogen is the ideal atom for the incoherent scattering of neutrons, since the cross section for incoherent scattering is large relative to its own coherent scattering cross section and the cross sections of most atoms likely to be encountered in natural materials. Hydrogen often occurs as part of a molecule, such as water or methane. Consider first a single hydrogen atom in a molecule. Its instantaneous absolute position, $\mathbf{r}(t)$, can be written as

$$\mathbf{r}(t) = \mathbf{R}(t) + \mathbf{d}(t) + \mathbf{u}(t) \quad (53),$$

where $\mathbf{R}(t)$ is the instantaneous position of the centre-of-mass of the molecule (not to be confused with the mean position, for which we used the same symbol earlier), $\mathbf{d}(t)$ is the instantaneous position of the hydrogen atom with respect to the molecular centre-of-mass assumed to have constant magnitude but variable direction, and $\mathbf{u}(t)$ is the vibrational displacement of the atom from its 'mean' position (magnitudes $d \gg$ u). Note that we are taking account of the fact that the motions associated with the vibrational displacement $\mathbf{u}(t)$ are much faster than the rotational motion of the molecule, which is why we can treat the behaviour of the bond vector $\mathbf{d}(t)$ separately from the vibrational displacement $\mathbf{u}(t)$, equation (14).

We are fundamentally interested in the quantity $\langle \exp(i\mathbf{Q}\cdot[\mathbf{r}(t) - \mathbf{r}(0)]) \rangle$ (equation 14). This can be written as

$$\langle \exp(i\mathbf{Q}\cdot[\mathbf{r}(t) - \mathbf{r}(0)]) \rangle =$$

$$\langle \exp(i\mathbf{Q}\cdot[\mathbf{R}(t) - \mathbf{R}(0)]) \times \exp(i\mathbf{Q}\cdot[\mathbf{d}(t) - \mathbf{d}(0)])$$

$$\times \exp(i(\mathbf{Q}\cdot[\mathbf{u}(t) - \mathbf{u}(0)]) \rangle \quad (54).$$

If the translational, rotational and vibrational motions are not coupled, we can perform the averages on the three exponential terms separately, obtaining the total function (with self-explanatory notation),

$$F_{inc}^{tot}(\mathbf{Q},t) = F_{inc}^{trans}(\mathbf{Q},t) \times F_{inc}^{rot}(\mathbf{Q},t) \times F_{inc}^{vib}(\mathbf{Q},t) \quad (55).$$

When we take the Fourier transforms, we have the convolution of the incoherent inelastic scattering functions for the three types of motion:

$$S_{inc}^{tot}(\mathbf{Q},\omega) = S_{inc}^{trans}(\mathbf{Q},\omega) \otimes S_{inc}^{rot}(\mathbf{Q},\omega) \otimes S_{inc}^{vib}(\mathbf{Q},\omega) \quad (56).$$

In practice the different types of motion within crystals occur on sufficiently different time scales that the effects of the convolution do not cause any major problems in the analysis of incoherent neutron scattering data – these problems mostly occur in the study of molecular fluids.

4.2 Atomic diffusion

Incoherent neutron scattering can be used to provide information about the motions of individual atoms as they diffuse through a crystalline or liquid medium, which are described by the time dependence of $\mathbf{R}$. One example is the diffusion of hydrogen atoms in metals such as palladium. Atomic hydrogen enters the metal in interstitial sites, and is able to jump from site to site rather quickly. Another example is diffusion within molecular fluids. For these cases incoherent neutron scattering can provide information about the time constants for the diffusion and the diffusion pathways.

Consider first the case of *isotropic diffusion*, as in a simple liquid or as a first approximation to a crystal. In this case there is no potential to worry about. The probability distribution function $G(\mathbf{r}(t),\mathbf{r}(0))$ in equation (15), which we rewrite as $G(\mathbf{r},t)$, $\mathbf{r} = \mathbf{r}(t) - \mathbf{r}(0)$, is determined by the standard rate equation for diffusion (Fick's second law):

$$\frac{\partial G}{\partial t} = D\nabla^2 G \quad (57),$$

where D is the diffusion constant. This has the solution

$$G(\mathbf{r},t) = (4\pi Dt)^{-3/2} \exp\left(-r^2 / 4Dt\right) \quad (58),$$

where r is the modulus of $\mathbf{r}$. This solution is consistent with the boundary conditions:

$$G(\mathbf{r},0) = \delta(\mathbf{r})$$

$$\int G(\mathbf{r},t)\mathrm{d}\mathbf{r} = 1 \text{ for all } t \quad (59).$$

Substituting the solution into the equation for the intermediate scattering function (noting that for the present case the probability $p(\mathbf{r})$ is constant for all values of $\mathbf{r}$) leads to the result

$$F_{\mathrm{inc}}(\mathbf{Q},t) = \exp\left(-DQ^2t\right) \quad (60),$$

where Q is the modulus of $\mathbf{Q}$, and N is the number of atoms. Fourier transformation gives the final incoherent scattering function for our example:

$$S_{\mathrm{inc}}(\mathbf{Q},\omega) = \frac{1}{\pi}\frac{DQ^2}{(DQ^2)^2 + \omega^2} \quad (61).$$

The final scattering function for the case of isotropic diffusion is thus a single Lorentzian function centred on zero frequency with a frequency width that varies with Q^2 and amplitude that varies as Q^{-2}. The width is also proportional to the diffusion constant D, and hence the time constant associated with the diffusion. In general this peak is narrow (by some orders of magnitude) compared to phonon frequencies, and the term *quasi-elastic scattering* has been coined to describe such scattering. *Incoherent quasi-elastic neutron scattering* (IQNS) probes time scales that are so much slower than the time scales for phonon motion that special instruments have to be designed for these experiments. The typical resolution of an IQNS instrument will range from 10^8 to 10^{10} Hz, which is much finer than the typical value of 10^{11} Hz for a triple-axis spectrometer.

For crystalline media, the basic model needs to be modified in two ways. Firstly we need to take account of the position-dependent potential, and secondly we also need to take account of the fact that the diffusion constant will in general be a tensor rather than a single value, reflecting the fact that the diffusion will be easier in some directions than in others. The mathematics gets far beyond the scope of this book at this point, but three points should be noted. Firstly, the general form of the Q^2-dependent Lorentzian term is usually recovered from more complicated treatments, although the general solution may contain a superposition of several Lorentzian functions. However, by analysing data obtained over a range of values of Q, particularly as Q tends to small values, the behaviour of the individual components (particularly the lowest-order component) can be deduced. Secondly, because the diffusion constant is a tensor and hence anisotropic, the scattering function will depend on the orientation of $\mathbf{Q}$ rather than only upon its magnitude. Work with powders will therefore give an average over all orientations, which may not matter if it is known that diffusion is only significant along one direction in the crystal. Thirdly, the existence of a periodic potential (as found in a crystal) leads to the existence of *elastic incoherent scattering* when $\mathbf{Q}$ is equal to a reciprocal lattice vector. This elastic scattering contains information about the strength of the periodic potential. In many cases the effect of the potential is to cause the diffusing atoms to be able to exist only on well-defined sites within the crystal, and the diffusion proceeds by the atoms jumping between these sites. In the limit where the time taken to jump is much less than the average time that an atom remains in a site standard jump diffusion models can be used in the interpretation of the quasi-elastic scattering.

The incoherent scattering method has not yet been used for studies of diffusion in mineral sciences. The main applications could be for the study of hydrogen diffusion in minerals and fluids, for which there have been extensive measurements on metals. Bée (1988) describes many of the experimental and theoretical details, including the development of the formalism beyond the 'trivial' case described above.

4.3 Collective vibrations and vibrational spectroscopy

Having remarked that the frequency regime for the observation of translational diffusion is much lower than for phonons, we should also note that the time dependence of both $\mathbf{R}$ and $\mathbf{u}$ contains a contribution from the phonons. We can broadly interpret the time-dependence of $\mathbf{R}$ as arising from lattice vibrations in which the molecules move as rigid bodies, giving the lower-frequency modes, and the time-dependence of $\mathbf{u}$ as arising from the higher-frequency internal vibrations of the molecules. These motions can be measured if the incoherent spectrum is recorded over the appropriate frequency range. The resultant form of $S_{\mathrm{inc}}(\omega)$, when averaged over Q, gives the phonon density of states weighted by the relevant incoherent neutron cross sections. For systems containing hydrogen, the spectrum will be dominated by the motions of the hydrogen atoms.

Vanadium is an unusual system in that the scattering lengths for the two spin states are of opposite sign and nearly equal magnitude, leading to a very small coherent scattering length (as a result of which vanadium is very suitable for making sample holders for neutron scattering, as it will not contribute any Bragg scattering to the measured spectrum), but to a reasonably large incoherent scattering cross section (see Fig. 1). The incoherent scattering from vanadium is often used to calibrate neutron scattering instruments. Vanadium has therefore been used for the measurement of the phonon density of states using incoherent neutron scattering.

The fact that hydrogen has a large incoherent cross section means that incoherent neutron scattering can be used for vibrational spectroscopy. We have previously noted that there is not a significant wave vector dependence for the high frequency modes, which means that the phonon modes measured as a density of states will have sharp peaks and will not require a good average over scattering vectors. The advantage of incoherent neutron scat-

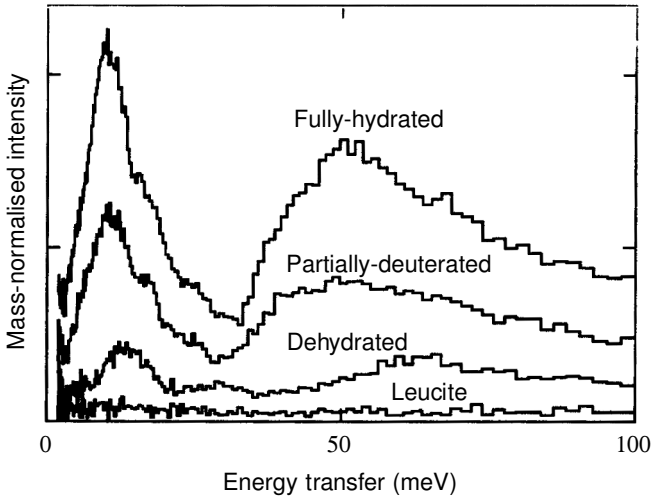

Fig. 12. Incoherent inelastic neutron scattering from samples of analcime with various degrees of hydration and compared with scattering from leucite. The data were obtained from the TFXA crystal-analyser spectrometer at the ISIS spallation neutron source (unpublished data of C.M.B. Line and M.T. Dove, reported in Line, 1995).

tering as a tool for vibrational spectroscopy over light scattering methods is that there are no selection rules that cause modes to be unobservable.

Although the phonon modes have a much higher frequency than the energies associated with translational diffusion and rotational motions, the quasi-elastic scattering is convoluted with the vibrational spectrum. In practice this convolution gives rise to a Debye–Waller prefactor to the correct expression for the quasi-elastic intensity, exactly as in the case of coherent neutron scattering.

An example of the information that can be obtained using vibrational incoherent neutron spectroscopy is shown in Fig. 12, which gives the spectra for analcime in various states of hydration and a comparison with the closely related structure leucite. The fact that the intensities of the spectra are reduced as the hydrogen content of the samples is lowered indicates that the spectra are dominated by the incoherent scattering from the hydrogen atoms. The spectra have two main features. The *first* is a peak around 15 meV, which is due to whole molecular librations. The *second* feature is a broader peak around 50 meV. This arises from the coupling of the water molecules to the vibrations of the network of SiO_4 and AlO_4 tetrahedra. Similar studies have been carried out on bassanite, gypsum and cordierite (Winkler & Hennion, 1994; Winkler, 1996) and small-pored zeolites (Line & Kearley, 2000).

4.4 Rotational motions

As a molecule rotates about its centre-of-mass, the relative positions of the hydrogen atoms, $\mathbf{d}(t)$, move over the surface of a sphere of constant radius d. This motion is called *rotational diffusion*, as the end point of the vector $\mathbf{d}$ diffuses over the surface of the sphere. We will first consider the simple illustrative case of isotropic rotational diffusion of an atom – this is a good model for a molecular liquid, and is also a good first-approximation for systems such as crystalline methane just below the melting temperature, where experiments indicate that although the positions of the molecules are ordered on a lattice, the molecules are freely rotating. We can define the orientation of $\mathbf{d}$ by the polar angle $\boldsymbol{\Omega} = (\theta,\phi)$. The relevant probability distribution function, G, for equation (15) is now a function of $\boldsymbol{\Omega}(t)$ and $\boldsymbol{\Omega}(0)$. Formally $G(\boldsymbol{\Omega}(t),\boldsymbol{\Omega}(0)$ is the probability of finding the bond orientation at $\boldsymbol{\Omega}(t)$ at time t if it has the orientation $\boldsymbol{\Omega}(0)$ at time 0, and it follows a similar rate law to the case of translation diffusion:

$$\frac{\partial G}{\partial t} = D_{\mathrm{R}} \nabla^2_{\Omega} G \qquad (62),$$

where D_{R} is the rotational diffusion constant, and its inverse gives the time constant for reorientational motions. The differential operator in spherical coordinates is given as

$$\nabla^2_{\Omega} = \frac{1}{\sin\theta}\frac{\partial}{\partial\theta}\left(\sin\theta\frac{\partial}{\partial\theta}\right) + \frac{1}{\sin^2\theta}\frac{\partial^2}{\partial\phi^2} \qquad (63).$$

As for the case of translational diffusion, the apparent simplicity of the rate equation belies the complexity of the solution. And, as before, we can only quote the solution (Bée, 1988):

$$G(\boldsymbol{\Omega}(t),\boldsymbol{\Omega}(0)) = 4\pi\sum_{\ell=0}^{\infty}\exp(-D_{\mathrm{R}}\ell(\ell+1)t)\sum_{m=-\ell}^{+\ell} Y_m^{\ell}(\boldsymbol{\Omega}(t))Y_m^{\ell *}(\boldsymbol{\Omega}(0)) \qquad (64),$$

where the functions $Y_m^{\ell}(\boldsymbol{\Omega})$ are the normal *spherical harmonic*s (the * indicates the complex conjugates). Substitution of this expression generates the intermediate scattering function:

$$F_{\mathrm{inc}}(\mathbf{Q},t) \propto j_0^2(Qd) + \frac{1}{\pi}\sum_{\ell=1}^{\infty}(2\ell+1)j_{\ell}^2(Qd)\exp(-D_{\mathrm{R}}\ell(\ell+1)t \qquad (65),$$

where the functions j_{ℓ} are the regular *Bessel functions*. The Fourier transform gives the incoherent scattering function:

$$S_{\mathrm{inc}}(\mathbf{Q},\omega) \propto j_0^2(Qd)\delta(\omega) + \frac{1}{\pi}\sum_{\ell=1}^{\infty}(2\ell+1)j_{\ell}^2(Qd)\frac{D_{\mathrm{R}}\ell(\ell+1)}{(D_{\mathrm{R}}\ell(\ell+1))^2+\omega^2} \qquad (66),$$

where $\delta(\omega)$ is the Dirac delta function. This equation has two components. The first ($\ell = 0$) is an elastic peak centred on $\omega = 0$, which will be considered in more detail below. The second is a superposition of Lorentzian peaks, with widths that are independent of Q. The lowest order term in this second component ($\ell = 1$) has a width equal to $2D_{\mathrm{R}}$, and higher order terms have larger widths. On the other hand, the amplitudes of the quasi-elastic components are dependent on Q through the Bessel functions.

The theory needs to be modified to take account of orientational crystal potentials. For example, the ammonium molecular ion, NH_4^+, is known to undergo frequent reorientations in the CsCl form of ammonium chloride. The electrostatic potentials are sufficiently anisotropic to ensure that the N–H bonds lie along the $\langle 111 \rangle$ directions –

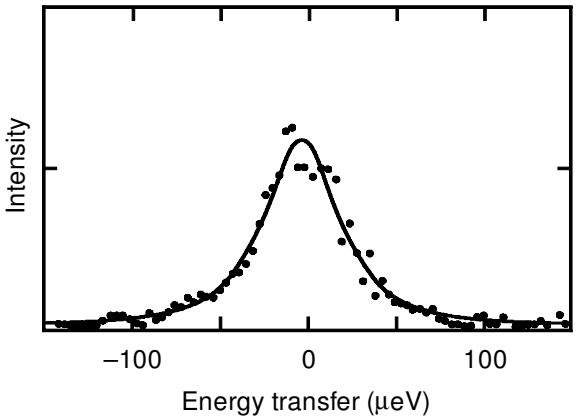

Fig. 13. Quasi-elastic scattering spectrum for analcime. The curve is a Lorentzian of halfwidth 30 μeV convoluted with the resolution function. The data were obtained from the high-resolution back-scattering IRIS spectrometer at the ISIS spallation neutron source (Line *et al.*, 1994).

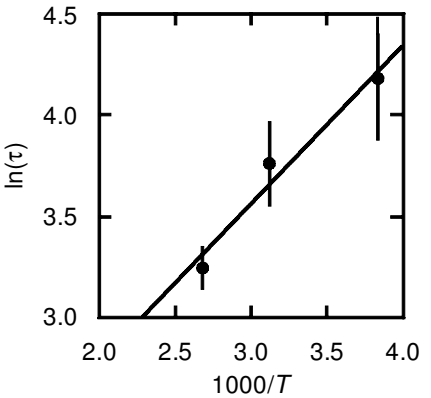

Fig. 14. Arrhenius plot of the relaxation time for water reorientations in analcime obtained from the quasi-elastic spectra (Line *et al.*, 1994).

there are effectively two independent orientations of the ammonium ion on this site. This results in a more complicated scattering function, but the essential details – namely the elastic and the quasielastic components – are preserved. A complete description of the theory for a range of complex situations is given by Bée (1988).

It is often found that the temperature dependence of the width of the quasi-elastic component follows an Arrhenius relation,

$$\tau^{-1} = D = D_0 \exp(-E_R/RT) \qquad (67),$$

where E_R is the activation energy associated with the rotational motion.

An example of a quasi-elastic spectrum associated with rotations of water molecules in analcime is shown in Fig. 13 (Line *et al.*, 1994). This spectrum has had the elastic peak subtracted out. The important point from the Fig. is the energy range of the quasi-elastic spectrum, which is much lower than the energy range of vibrational excitations seen in Fig. 12. It is clear that high resolution is required for quasi-elastic scatterning experiments – the various types of technology are reviewed by Bée (1988).

The widths of the quasi-elastic spectra for analcime have been shown to be constant with Q, and to increase on heating. These features are consistent with rotational motions that become faster with increasing temperature. The Arrhenius plot of the relaxation time (the inverse of the width of the quasi-elastic spectrum) is shown in Fig. 14. The fit to the data gave an activation energy of $E_R/R = 780 \pm 200$ K (Line *et al.*, 1994).

4.5 Elastic incoherent scattering function

The quasi-elastic incoherent scattering gives a means of measuring the time constants for rotational diffusion. The elastic component, on the other hand, gives information concerning the positions of the hydrogen atoms.

The elastic component is used to define the *elastic incoherent structure factor* (EISF) $I_{EISF}(Q)$:

$$I_{EISF}(Q) = \frac{S_{el}(Q)}{S_{el}(Q) + S_{qe}(Q)} \qquad (68),$$

where $S_{el}(Q)$ is the intensity of the incoherent elastic peak, and $S_{qe}(Q)$ is the intensity of the quasi-elastic peak integrated over all energies. The integration of $S(\mathbf{Q},\omega)$ over all frequencies is equal to $F(\mathbf{Q},0)$. Thus the elastic component $S_{el}(Q)$ is given by the $\ell = 0$ term, and the quasi-elastic term $S_{QE}(Q)$ is given by the terms for $\ell \geq 1$. Given that $j_\ell(x)$ tends to the value 0 when $x = 0$ for all values of $\ell \neq 0$, we see that $I_{EISF}(Q)$ has a maximum value of 1 at $Q = 0$. We also note that the form of $I_{EISF}(Q)$ is determined only from geometric properties – there is no dependence on the time constants and hence no dependence on temperature, apart from any dependence of the structure on temperature.

For isotropic rotational motions of molecules, the EISF has the simple form

$$I_{EISF}(Q) = \frac{\sin Qr}{Qr} \qquad (69),$$

where r is the radius of the molecule. The model of isotropic rotational diffusion is usually not realistic for most types of rotational diffusion. Usually the rotational diffusion is influenced by the rotational potential experienced by the molecules, which will have the same symmetry as the local site. The development of a model for the rotational diffusion from which the form of $I_{EISF}(Q)$ can be calculated is usually extremely difficult, and analytical solutions only occur for idealised cases such as uniaxial rotation in an n-fold potential or for jump motions between a small number of well-defined orientations. Inevitably it is necessary to use a model that is an oversimplification of the real situation, but given that even a simple model will capture the essential dynamic and geometric aspects of the motion this may not be too much of a problem. In the interpretation of measurements of $I_{EISF}(Q)$ it is common to compare the experimental data with the predicted function obtained from the model, in order to assess whether the model is correct. In many cases the calculated form of

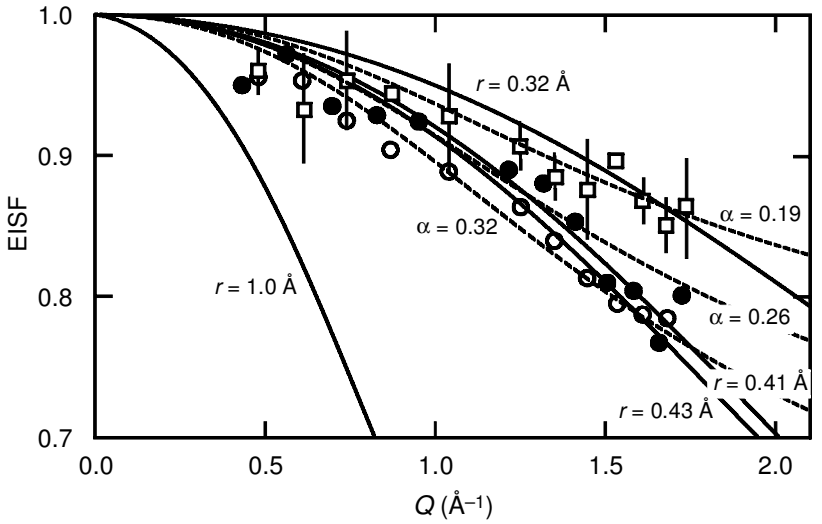

Fig. 15. The EISF for analcime obtained at three temperatures (squares are 260 K, filled circles are 320 K, and open circles are 373 K). The curves marked with a value for the molecular radius **r** are fits with the model EISF for isotropic rotation with a variable effective radius for rotation. The curves marked with a value of α are for a model EISF with fixed rotation radius (0.88 Å) but with varying fraction α of the molecules that participate in the rotational motions (Line *et al.*, 1994).

$I_{\mathrm{EISF}}(Q)$ does not have any free parameters – the parameters in the model are quantities such as the bond lengths, which are known in advance.

The biggest problem in extracting $I_{\mathrm{EISF}}(Q)$ from experimental data is accounting for multiple scattering. Because the incoherent cross section for hydrogen is so large, there is always a high probability that any neutron will be scattered more than once whilst travelling through the sample. The effect of this will be to reduce the size of the elastic component, and hence of $I_{\mathrm{EISF}}(Q)$. The existence of multiple scattering will be revealed if the extracted form of $I_{\mathrm{EISF}}(Q)$ tends towards a limiting value lower than 1 for small values of Q. Complicated methods are available for accounting for multiple scattering, but a better approach is to reduce the size of multiple scattering in the experiment by the use of thin samples, and to measure spectra only for transmission with short path lengths or reflection. It is the problem of multiple scattering that has discouraged the use of single crystal samples, given that the best single crystal samples will ideally be in the form of a thin flat plate with the large faces being coincident with a crystal plane of interest. It is clear that there should be a higher information content if single crystals are used, in that for rotational diffusion in an anisotropic potential it is expected that the elastic incoherent structure factor will have a dependence on the direction of the scattering vector **Q** as well as on its magnitude. Despite the experimental difficulties, some measurements of $I_{\mathrm{EISF}}(Q)$ have been obtained from single crystals.

The measured EISF for analcime is shown in Fig. 15 (Line *et al.*, 1994). The data are fitted by two types of curves. The *first* is a standard isotropic rotational EISF as given by equation (69), with the effective radius being fitted at each temperature and reproduced in the figure. The *second* type of curve is again based on the standard isotropic rotational EISF with a molecular radius of 0.88 Å, but allowing for the possibility that only a fraction α of the water molecules participate in the rotational motions. The data cannot give a judgement as to the most appropriate model. For small molecules such as water, it is necessary to extend the measurements to higher values of Q, but there are then difficulties with overlapping Bragg peaks.

The only other study of quasi-elastic scattering from rotations of water molecules in minerals was carried out by Winkler *et al.* (1994) on hydrous cordierite. There is considerable scope for developing this line of work with minerals that contain molecular water. Quasielastic scattering experiments provide unique information about the dynamics of water molecules, both in respect to the time scales for motion and the geometric changes associated with these motions.

6. Summary

The main point that I have sought to convey in this review article is that neutron scattering has a tremendous versatility that can be exploited for studies of mineral behaviour. This versatility is being constantly extended as new neutron sources and new instrumentation come into operation. The focus of this review has been on how this versatility arises from the fact that the characteristic length and energy scales of neutron beams are closely matched to those of the atoms in condensed matter, enabling neutron scattering to provide information about structure and dynamics. These two aspects are encapsulated within the general formulation of the neutron scattering law. The versatility of neutron scattering is further enhanced by the unique possibility to separate out both coherent and incoherent scattering.

We have described in detail a selection of the neutron scattering techniques that are routinely used in the wider science communities and which have been more-or-less picked up by the Earth and Mineral Sciences community. These include coherent inelastic scattering for single crystals and polycrystalline samples, diffraction on powders and single crystals, single-crystal diffuse scattering, total scattering from polycrystalline materials, vibrational incoherent scattering, and incoherent quasi-elastic scattering. The review also touches on magnetic scattering (diffraction

and inelastic) and small-angle scattering, both of which are ripe for exploitation. This review has not touched on some other applications, such as surface reflectometry and deep inelastic scattering (otherwise known as neutron Compton scattering), which again are ripe for exploitation.

Acknowledgements: I am pleased to acknowledge collaboration in neutron scattering experiments with many people over the past few years. These include Brian Powell and Ian Swainson (Chalk River), David Keen and Mark Harris (ISIS), Mark Hagen (Keele), Björn Winkler (Kiel), Christina Line, Matthew Tucker and Simon Redfern (Cambridge). I am grateful for financial support from EPSRC to support these collaborations.

References

Artioli, G. (2002): Single crystal neutron diffraction. *Eur. J. Mineral.*, **14**, 233–239.

Artioli, G., Rinaldi, R., Wilson, C.C., Zanazzi, P.F. (1995a): Single-crystal pulsed-neutron diffraction of a highly hydrous beryl. *Acta Cryst. B*, **51**, 733–737.

—, —, —, — (1995b): High–temperature Fe–Mg cation partitioning in olivine: *in situ* single-crystal neutron-diffraction study. *Am. Mineral.*, **80**, 197–200.

Artioli, G., Besson J.M., Dove, M.T., Geiger, C.A., Rinaldi, R., Schaefer, W. (1996a): Earth Sciences. *in* "Scientific Prospects for Neutron Scattering with Present and Future Sources (ESF Framework Studies into Large Research Facilities)" ESF (Strasbourg), 94–108.

Artioli, G., Pavese, A., Moze, O. (1996b): Dispersion relations of acoustic phonons in pyrope garnet: Relationship between vibrational properties and elastic constants. *Am. Mineral.*, **81**, 19–25.

Artioli, G., Pavese, A., Stahl, K., McMullan, R.K. (1997): Single-crystal neutron-diffraction study of pyrope in the temperature range 30–1173 K. *Can. Mineral.*, **35**, 1009–1019.

Ashcroft, N.W. & Mermin, N.D. (1976): Solid State Physics. Holt, Rinehart and Winston, New York. 826 p.

Bée, M. (1988): Quasielastic neutron scattering: principles and applications in solid state chemistry, biology, and materials science. Adam Hilger, Bristol. 437 p.

Besson, J.M. & Nelmes, R.J. (1995), New developments in neutron-scattering methods under high pressure with the Paris-Edinburgh cells. *Physica B*, **213**, 31–36.

Bethke, J., Dolino, G., Eckold, G., Berge, B., Vallade, M., Zeyen, C.M.E., Hahn, T., Arnold, H., Moussa, F. (1987): Phonon dispersion and mode coupling in high–quartz near the incommensurate phase–transition. *Europhys. Lett.*, **3**, 207–212.

Bethke, J., Eckold, G., Hahn, T. (1992): The phonon dispersion and lattice dynamics of α-$AlPO_4$: an inelastic neutron–scattering study. *J. Phys.: Condensed Matter*, **4**, 5537–5550.

Boysen, H. (1990): Neutron scattering and phase transitions in leucite. *in* "Phase transitions in ferroelastic and co-elastic crystals", Cambridge University Press, Cambridge, 334–349.

Boysen, H., Dorner, B., Frey, F., Grimm, H. (1980): Dynamic structure determination for two interacting modes at the M point in α- and β-quartz by inelastic neutron scattering. *J. Phys. C: Solid State Phys.*, **13**, 6127–6146.

Castellano, E.E. & Main, P. (1985): On the classical interpretation of thermal probability ellipsoids and the Debye–Waller factor. *Acta Cryst. A*, **41**, 156–157.

Catti, M., Ferraris, G., Hull, S., Pavese, A. (1994): Powder neutron-diffraction study of 2M1 muscovite at room pressure and at 2 GPa. *Eur. J. Mineral.*, **6**, 171–178.

—, —, —, — (1995): Static compression and H-disorder in brucite, $Mg(OH)_2$, to 11 GPa – a powder neutron-diffraction study. *Phys. Chem. Minerals*, **22**, 200–206.

Chaplot, S.L., Choudhury, N., Ghose, S., Rao, M.N., Mittal, R., Goel, P. (2002): Inelastic neutron scattering and lattice dynamics of minerals. *Eur. J. Mineral.*, **14**, 291–329.

Choudhury, N., Ghose, S., Chowdhury, C.P., Loong, C.K., Chaplot, S.L. (1998): Lattice dynamics, Raman spectroscopy, and inelastic neutron scattering of orthoenstatite $Mg_2Si_2O_6$. *Phys. Rev. B*, **58**, 756–765.

Coey, J.M.D. & Ghose, S. (1985): Magnetic order in hedenbergite, $CaFeSi_2O_6$. *Solid State Comm.*, **53**, 143–145.

Cowley, E.R. & Pant, A.K. (1970): Lattice dynamics of calcite. *Phys. Rev.*, **B8**, 4795–4800.

Dolino, G., Berge, B., Vallade, M., Moussa, F. (1992): Origin of the incommensurate phase of quartz .1. Inelastic neutron-scattering study of the high-temperature β-phase of quartz. *J. Phys. I*, **2**, 1461–1480.

Dove, M.T. (1993): Introduction to lattice dynamics. Cambridge University Press, Cambridge. 258 p.

Dove, M.T. & Keen, D.A. (1999): Atomic structure of disordered materials. *in* "Microscopic properties and processes in minerals" (ed. C.R.A. Catlow and K. Wright), 371–387.

Dove, M.T. & Powell, B.M. (1989): Neutron diffraction study of the tricritical orientational order/disorder phase transition in calcite at 1260 K. *Phys. Chem. Minerals*, **16**, 503–507.

Dove, M.T., Hagen, M.E., Harris, M.J., Powell, B.M., Steigenberger, U., Winkler, B. (1992): Anomalous inelastic neutron scattering from calcite. *J. Phys.: Condensed Matter*, **4**, 2761–2774.

Dove, M.T., Keen, D.A., Hannon, A.C., Swainson, I.P. (1997): Direct measurement of the Si–O bond length and orientational disorder in β-cristobalite. *Phys. Chem. Minerals*, **24**, 311–317.

Dove, M.T., Craig, M.S., Keen, D.A., Marshall, W.G., Redfern, S.A.T., Trachenko, K.O., Tucker, M.G. (2000a): Crystal structure of the high-pressure monoclinic phase-II of cristobalite, SiO_2. *Min. Mag.*, **64**, 569–576.

Dove, M.T., Hammonds, K.D., Harris, M.J., V Heine, Keen, D.A., Pryde, A.K.A., Trachenko, K., Warren, M.C. (2000b): Amorphous silica from the Rigid Unit Mode approach. *Min. Mag.*, **64**, 377–388.

Dove, M.T., Tucker, M.G., Keen, D.A. (2002): Neutron total scattering method: simultaneous determination of long-range and short-range order in disordered materials. *Eur. J. Mineral.*, **14**, 331–348.

Dove, M.T., Trachenko, K.O., Tucker, M.G., Keen, D.A. (2000c): Rigid Unit Modes in framework structures: theory, experiment and applications. *Rev. Mineral. Geochem.*, **39**, 1–33.

Fowler, P.H. & Taylor, A.D. (1987): Temperature imaging using epithermal neutrons. Rutherford Appleton Laboratory Report RAL-87-056.

Frost, J.C., Meehan, P., Morris, S.R., Ward, R.C, Mayers, J. (1989): Non-intrusive temperature-measurement of the components of a working catalyst by neutron resonance radiography. *Catalysis Letters*, **2**, 97–104.

Ghose, S., Hewat, A.W., Marezio, M. (1984): A neutron powder diffraction study of the crystal and magnetic–structures of ilvaite from 305 K to 5 K: a mixed-valence iron silicate with an electronic–transition. *Phys. Chem. Minerals*, **11**, 67–74.

Ghose, S., Schomaker, V., Mcmullan, R.K. (1986): Enstatite, $Mg_2Si_2O_6$: a neutron diffraction refinement of the crystal structure and a rigid-body analysis of the thermal vibration. *Zeit. Kristall.*, **176**, 159–175.

Ghose, S., Hewat, A.W., Pinkney, M. (1990): A powder neutron diffraction study of magnetic phase–transitions and spin frustration in ilvaite, a mixed-valence iron silicate showing a semiconductor–insulator transition. *Solid State Comm.*, **74**, 413–418.

Ghose, S., Hastings, J.M., Choudhury, N., Chaplot, S.L., Rao, K.R. (1991): Phonon dispersion relation in fayalite, Fe_2SiO_4. *Physica B*, **174**, 83–86.

Ghose, S., Mcmullan, R.K., Weber, H.P. (1993): Neutron diffraction studies of the $P\bar{1}$–$I\bar{1}$ transition in anorthite, $CaAl_2Si_2O_8$, and the crystal structure of the body-centered phase at 514 K. *Zeit. Kristall.*, **204**, 215–237.

Graetsch, H. & Ibel, K. (1997): Small angle neutron scattering by opals. *Phys. Chem. Minerals*, **24**, 102–108.

Hammonds, K.D., Dove, M.T., Giddy, A.P., Heine, V., Winkler, B. (1996): Rigid unit phonon modes and structural phase transitions in framework silicates. *Am. Mineral.*, **81**, 1057–1079.

Harris, M.J., Cowley, R.A., Swainson, I.P., Dove, M.T. (1993): Observation of lattice melting at the ferroelastic phase transition in Na_2CO_3. *Phys. Rev. Lett.*, **71**, 2939–2942.

Harris, M.J., Dove, M.T., Godfrey, K.W. (1996): A single crystal neutron scattering study of lattice melting in ferroelastic Na_2CO_3. *J. Phys.: Condensed Matter.*, **8**, 7073–7084.

Harris, M.J., Dove, M.T., Swainson, I.P., Hagen, M.E. (1998a): Anomalous dynamical effects in calcite, $CaCO_3$. *J. Phys.: Condensed Matter.*, **10**, L423–429.

Harrison, R.J. & Redfern, S.A.T. (2001): Short- and long-range ordering in the ilmenite-hematite solid solution. *Phys. Chem. Minerals*, **28**, 399–412.

Harrison, R.J., Redfern, S.A.T., O'Neill, H.S.C. (1998): The temperature dependence of the cation distribution in synthetic hercynite ($FeAl_2O_4$): from *in situ* neutron structure refinements. *Am. Mineral.*, **83**, 1092–1099.

Harrison, R.J., Dove, M.T., Knight, K.S., Putnis, A. (1999): *In situ* neutron diffraction study of non–convergent cation ordering in the $(Fe_3O_4)_{1-x}(MgAl_2O_4)_x$ spinel solid solution. *Am. Mineral.*, **84**, 555–563.

Harrison, R.J., Redfern, S.A.T., Smith, R.I. (2000): *In–situ* study of the $R\bar{3}$ *to* $R\bar{3}c$ phase transition in the ilmenite–hematite solid solution using time-of-flight neutron powder diffraction. *Am. Mineral.*, **85**, 194–205.

Henderson, C.M.B., Knight, K.S., Redfern, S.A.T., Wood, B.J. (1996): High-temperature study of octahedral cation exchange in olivine by neutron powder diffraction. *Science*, **271**, 1713–1715.

Kagi, H., Parise, J.B., Cho, H., Rossman, G.R., Loveday, J.S. (2000): Hydrogen bonding interactions in phase A $[Mg_7Si_2O_8(OH)_6]$ at ambient and high pressure. *Phys. Chem. Minerals*, **27**, 225–233.

Keen D.A. (2001): A comparison of various commonly used correlation functions for describing total scattering. *J. Appl. Cryst.*, **34**, 172–177.

Keen, D.A. & Dove, M.T. (1999): Comparing the local structures of amorphous and crystalline polymorphs of silica. *J. Phys.: Condensed Matter*, **11**, 9263–9273.

—, — (2000): Total scattering studies of silica polymorphs: similarities in glass and disordered crystalline local structure. *Min. Mag.*, **64**, 447–457.

Knight, K.S. (2000): A high temperature structural phase transition in crocoite ($PbCrO_4$): at 1068 K: crystal structure refinement at 1073 K and thermal expansion tensor determination at 1000 K. *Min. Mag.*, **64**, 291–300.

Lager, G.A. & von Dreele, R.B. (1996): Neutron powder diffraction study of hydrogarnet to 9.0 GPa. *Am. Mineral.*, **81**, 1097–1104.

Le Godec Y., Dove, M.T., Francis, D.J., Kohn, S.C., Marshall, W.G., Pawley, A.R., Price, G.D., Redfern, S.A.T., Rhodes, N., Ross, N.L., Schofield, P.F., Schooneveld, E., Syfosse, G., Tucker, M.G., Welch, M.D. (2001): Neutron diffraction at simultaneous high temperatures and pressures, with measurement of temperature by neutron radiography. *Min. Mag.*, **65**, 749–760.

Le Godec, Y., Dove, M.T., Redfern, S.A.T., Marshall, W.G., Tucker, M.G. Syfosse, G., Besson, J.M. (2002): A new high P-T cell for neutron diffraction up to 7 GPa and 2000 K with measurement of temperature by neutron radiography. *High Pressure Research*, **65**, 737-748.

Line, C.M.B. & Kearley, G.J. (2000): An inelastic incoherent neutron scattering study of water in small–pored zeolites and other water-bearing minerals. *J. Chem. Phys.*, **112**, 9058–9067.

Line, C.M.B., Winkler, B., Dove, M.T. (1994): Quasielastic incoherent neutron scattering study of the rotational dynamics of the water molecules in analcime. *Phys. Chem. Minerals*, **21**, 451–459.

Line, C.M.B., Dove, M.T., Knight, K.S., Winkler, B. (1996): The low-temperature behaviour of analcime, I: High-resolution neutron powder diffraction. *Min. Mag.*, **60**, 499–507.

Mayer, A.P. & Cowley, R.A. (1988): The continuous melting transition of a 3-dimensional crystal at a planar elastic instability. *J. Phys. C: Solid State Physics*, **21**, 4827–4834.

Mayers, J., Baciocco, G., Hannon, A.C. (1989): Temperature-measurement by neutron resonance radiography. *Nucl. Instr., Methods Phys. Research A*, **275**, 453–459.

Mittal, R., Chaplot, S.L., Parthasarathy, R., Bull, M.J., Harris, M.J. (2000a): Lattice dynamics calculations and phonon dispersion measurements of zircon, $ZrSiO_4$. *Phys. Rev. B*, **62**, 12089–12094.

Mittal, R., Chaplot, S.L., Choudhury, N., Loong, C.K. (2000b): Inelastic neutron scattering and lattice dynamics studies of almandine $Fe_3Al_2Si_3O_{12}$. *Phys. Rev. B*, **61**, 3983–3988.

Myer, H.-W., Marion, S., Sondergeld, P., Carpenter, M.A., Knight, K.S., Redfern, S.A.T., Dove, M.T. (2001): Displacive components of the phase transitions in lawsonite. *Am. Mineral.*, **86**, 566–577.

Nield, V.M. & Keen, D.A. (2001): Diffuse neutron scattering from crystalline materials. Oxford University Press, Oxford. 317 p.

Palmer, D.C., Dove, M.T., Ibberson, R.M., Powell, B.M. (1997): Structural behavior, crystal chemistry and phase transitions in substituted leucites. *Am. Mineral.*, **82**, 16–30.

Parise, J.B., Leinenweber, K., Weidner, D.J., Tan, K., von Dreele, R.B. (1993): Pressure-induced H-bonding – neutron-diffraction study of brucite, $Mg(OD)_2$, to 9.3 GPa. *Am. Mineral.*, **79**, 193–196.

Pavese, A. (2002): Neutron powder diffraction and Rietveld analysis: applications to crystal chemical studies of minerals at non-ambient conditions. *Eur. J. Mineral.*, **14**, 241–249.

Pavese, A., Ferraris, G., Prencipe, M., Ibberson, R. (1997): Cation site ordering in phengite 3T from the Dora–Maira massif (western Alps): a variable-temperature neutron powder diffraction study. *Eur. J. Mineral.*, **9**, 1183–1190.

Pavese, A., Artioli, G., Moze, O. (1998): Inelastic neutron scattering from pyrope powder: experimental data and theoretical calculations. *Eur. J. Mineral.*, **10**, 59–69.

Pavese, A., Artioli, G., Hull, S. (1999a): *In situ* powder neutron diffraction of cation partitioning *vs.* pressure in $Mg_{0.94}Al_{2.04}O_4$ synthetic spinel. *Am. Mineral.*, **84**, 905–912.

Pavese, A., Artioli, G., Russo, U., Hoser, A. (1999b): Cation partitioning versus temperature in $(Mg_{0.70}Fe_{0.23})Al_{1.97}O_4$ synthetic spinel by *in situ* neutron powder diffraction. *Phys. Chem. Minerals*, **26**, 242–250.

Pavese, A., Ferraris, G., Pischedda, V., Ibberson, R. (1999c): Tetrahedral order in phengite 2M(1): upon heating, from powder neutron diffraction, and thermodynamic consequences. *Eur. J. Mineral.*, **11**, 309–320.

Pavese, A., Artioli, G., Hoser, A. (2000a): $MgAl_2O_4$ synthetic spinel: cation and vacancy distribution as a function of temperature, from *in situ* neutron powder diffraction. *Zeit. Kristall.*, **215**, 406–412.

Pavese, A., Ferraris, G., Pischedda, V., Radaelli, P. (2000b): Further study of the cation ordering in phengite 3T by neutron powder diffraction. *Min. Mag.*, **64**, 11–18.

Payne, S.J., Harris, M.J., Hagen, M.E., Dove, M.T. (1997): A neutron diffraction study of the order–disorder phase transition in sodium nitrate. *J. Phys.: Condensed Matter*, **9**, 2423–2432.

Prencipe, M., Tribaudino, M., Pavese, A., Hoser, A., Reehuis, M. (2000): Single-crystal neutron diffraction investigation of diopside at 10 K. *Can. Mineral.*, **38**, 183–189.

Price, D.L., Ghose, S., Choudhury, N., Chaplot, S.L., Rao, K.R. (1991): Phonon density of states in fayalite, Fe_2SiO_4. *Physica B*, **174**, 87–90.

Rao, K.R., Chaplot, S.L., Choudhury, N., Ghose, S., Hastings, J.M., Corliss, L.M., Price, D.L. (1988): Lattice–dynamics and inelastic neutron–scattering from forsterite, Mg_2SiO_4: phonon dispersion relation, density of states and specific heat. *Phys. Chem. Minerals*, **16**, 83–97.

Rao, M.N., Chaplot, S.L., Choudhury, N., Rao, K.R., Azuah, R.T., Montfrooij, W.T., Bennington, S.M. (1999): Lattice dynamics and inelastic neutron scattering from sillimanite and kyanite Al_2SiO_5. *Phys. Rev. B*, **60**, 12061–12068.

Redfern S.A.T. (2002): Neutron powder diffraction of minerals at high pressures and temperatures: some recent technical developments and scientific applications. *Eur. J. Mineral.*, **14**, 251–261.

Redfern, S.A.T., Knight, K.S., Henderson, C.M.B., Wood, B.J. (1998): Fe–Mn cation ordering in fayalite–tephroite $(Fe_xMn_{1-x})_2SiO_4$ olivines: a neutron diffraction study. *Min. Mag.*, **62**, 607–615.

Redfern, S.A.T., Harrison, R.J., O'Neill, H.S.C., Wood, D.R.R. (1999): Thermodynamics and kinetics of cation ordering in $MgAl_2O_4$ spinel up to 1600°C from *in situ* neutron diffraction. *Am. Mineral.*, **84**, 299–310.

Redfern, S.A.T., Artioli, G., Rinaldi, R., Henderson, C.M.B., Knight, K.S., Wood, B.J. (2000): Octahedral cation ordering in olivine at high temperature. II: an *in situ* neutron powder diffraction study on synthetic $MgFeSiO_4$ (Fa50). *Phys. Chem. Minerals*, **27**, 630–637.

Redhammer, G.J., Roth, G., Paulus, W., Andre, G., Lottermoser, W., Amthauer, G., Treutmann, W., Koppelhuber-Bitschnau, B. (2001): The crystal and magnetic structure of Li-aegirine $LiFe^{3+}Si_2O_6$: a temperature-dependent study. *Phys. Chem. Minerals*, **28**, 337–346.

Reece, J.J., Redfern, S.A.T., Welch, M.D., Henderson, C.M.B. (2000): Mn–Mg disordering in cummingtonite: a high-temperature neutron powder diffraction study. *Min. Mag.*, **64**, 255–266.

Rinaldi, R. (2002): Neutron scattering in mineral sciences: preface. *Eur. J. Mineral.*, **14**, 195–202.

Rinaldi, R., Artioli, G., Wilson, C.C., McIntyre, G. (2000): Octahedral cation ordering in olivine at high temperature. I: *in situ* neutron single–crystal diffraction studies on natural mantle olivines (Fa12 and Fa10). *Phys. Chem. Minerals*, **27**, 623–629.

Samuelson, E.J. & Shirane, G. (1970): Inelastic neutron scattering investigation of spine waves and magnetic interactions in a-Fe_2O_3. *Physica Status Solidi*, **42**, 241–256.

Schäfer, W. (2002): Neutron diffraction applied to geological texture and stress analysis. *Eur. J. Mineral.*, **14**, 263–289.

Schmahl, W.W., Swainson, I.P., Dove, M.T., Graeme-Barber, A. (1992): Landau free energy and order parameter behaviour of the α–β phase transition in cristobalite. *Zeit. Kristall.*, **201**, 125–145.

Schober, H., Strauch, D., Dorner, B. (1993): Lattice dynamics of sapphire (Al_2O_3). *Zeit. Physik B: Condensed Matter*, **92**, 273–283.

Schofield, P.F., Stretton, I.C., Knight, K.S., Hull, S. (1997): Powder neutron diffraction studies of the thermal expansion, compressibility and dehydration of deuterated gypsum. *Physica B*, **234**, 942–944.

Schofield, P.F., Wilson, C.C., Knight, K.S., Stretton, I.C. (2000): Temperature related structural variation of the hydrous components in gypsum. *Zeit. Kristall.*, **215**, 707–710.

Ståhl, K. & Artioli, G. (1993): A neutron powder diffraction study of fully deuterated laumontite. *Eur. J. Mineral.*, **5**, 851–856.

Ståhl, K., Kvick, A., Ghose, S. (1987): A neutron diffraction and thermogravimetric study of the hydrogen bonding and dehydration behavior in fluorapophyllite, $KCa_4(Si_8O_{20})F.8H_2O$, and its partially dehydrated form. *Acta Cryst. B*, **43**, 517–523.

Strauch, D. & Dorner, B. (1993): Lattice dynamics of α-quartz .1. Experiment. *J. Phys.: Condensed Matter*, **5**, 6149–6154.

Swainson, I.P. & Dove, M.T. (1993): Low-frequency floppy modes in β-cristobalite. *Phys. Rev. Lett.*, **71**, 193–196.

Swainson, I.P., Dove, M.T., Schmahl, W.W., Putnis, A. (1992): Neutron powder diffraction study of the Åkermanite–Gehlenite solid solution series. *Phys. Chem. Minerals*, **19**, 185–195.

Swainson, I.P., Dove, M.T., Harris, M.J. (1995): Neutron powder diffraction study of the ferroelastic phase transition in sodium carbonate. *J. Phys.: Condensed Matter*, **7**, 4395–4417.

—, —, — (1997): The phase transitions in calcite and sodium nitrate. *Physica B*, **241**, 397–399.

Tucker, M.G., Dove, M.T., Keen, D.A. (2000a): Simultaneous analyses of changes in long-range and short-range structural order at the displacive phase transition in quartz. *J. Phys.: Condensed Matter*, **12**, L723–L730.

—, —, — (2000b): Direct measurement of the thermal expansion of the Si–O bond by neutron total scattering. *J. Phys.: Condensed Matter*, **12**, L425–L430.

Tucker, M.G., Keen, D.A., Dove, M.T. (2001a): A detailed structural characterisation of quartz on heating through the α–β phase transition. *Min. Mag.*, **65**, 489–507.

Tucker, M.G., Squires, M.D., Dove, M.T., Keen, D.A. (2001b): Dynamic structural disorder in cristobalite: Neutron total scattering measurement and Reverse Monte Carlo modelling. *J. Phys.: Condensed Matter*, **13**, 403–423.

Welch, M.D. & Knight, K.S. (1999): A neutron powder diffraction study of cation ordering in high–temperature synthetic amphiboles. *Eur. J. Mineral.*, **11**, 321–331.

Willis, B.T.M. & Pryor, A.W. (1975): Thermal vibrations in crystallography. Cambridge University Press, Cambridge.

Wilson, C.C. (1994): Structural studies of schultenite in the temperature range 125–324 K by pulsed single-crystal neutron diffraction: hydrogen ordering and structural distortions. *Min. Mag.*, **58**, 629–634.

Winkler, B. (1996): The dynamics of H_2O in minerals. *Phys. Chem. Minerals*, **23**, 310–318.

— (2002): Neutron sources and instrumentation. *Eur. J. Mineral.*, **14**, 225–232.

Winkler, B. & Buehrer, M. (1990): The lattice dynamics of andalusite: prediction and experiment. *Phys. Chem. Minerals*, **17**, 453–461.

Winkler, B. & Hennion, B. (1994): Low-temperature dynamics of molecular H_2O in bassanite, gypsum and cordierite investigated by high-resolution incoherent inelastic neutron–scattering. *Phys. Chem. Minerals*, **21**, 539–545.

Winkler, B., Coddens, G., Hennion, B. (1994): Movement of channel H_2O in cordierite observed with quasi–elastic neutron–scattering. *Am. Mineral.*, **79**, 801–808.

Winkler, B., Harris, M.J., Eccleston, R.S., Knorr, K., Hennion, B. (1997): Crystal field transitions in $Co_2[Al_4Si_5]O_{18}$ cordierite and $CoAl_2O_4$ spinel determined by neutron spectroscopy. *Phys. Chem. Minerals*, **25**, 79–82.

Winkler, B., Knorr, K., Kahle, A., Vontobel, P., Hennion, B., Lehmann, E., Bayon, G. (2002): Neutron imaging and neutron tomography as non-destructive tools to study bulk rock samples. *Eur. J. Mineral.*, **14**, 349–354.

Wood, I.G., David, W.I.F., Hull, S., Price, G.D. (1996): A high-pressure study of ε-FeSi, between 0 and 8.5 GPa, by time-of-flight neutron powder diffraction. *J. Appl. Cryst.*, **29**, 215–218.

Zhao, Y.S., von Dreele, R.B., Morgan, J.G. (1999): A high P-T cell assembly for neutron diffraction up to 10 GPa and 1500 K. *High Pressure Research*, **16**, 161–177.

Zhao, Y.S., Lawson, A.C., Zhang, J.Z., Bennett, B.I., von Dreele, R.B. (2000): Thermoelastic equation of state of molybdenum. *Phys. Rev. B*, **62**, 8766–8776.

Received 29 July 2001
Modified version received 12 September 2001
Accepted 6 November 2001